



THE UNIVERSITY *of* EDINBURGH

Edinburgh Research Explorer

## A coiled-coil affinity-based system for the controlled release of biofunctionalized gold nanoparticles from alginate hydrogels

### Citation for published version:

Roth, A, Murschel, F, Latreille, P-L, Martinez, V, Liberelle, B, Banquy, X & De Crescenzo, G 2019, 'A coiled-coil affinity-based system for the controlled release of biofunctionalized gold nanoparticles from alginate hydrogels', *Biomacromolecules*. <https://doi.org/10.1021/acs.biomac.9b00137>

### Digital Object Identifier (DOI):

[10.1021/acs.biomac.9b00137](https://doi.org/10.1021/acs.biomac.9b00137)

### Link:

[Link to publication record in Edinburgh Research Explorer](#)

### Document Version:

Peer reviewed version

### Published In:

Biomacromolecules

### General rights

Copyright for the publications made accessible via the Edinburgh Research Explorer is retained by the author(s) and / or other copyright owners and it is a condition of accessing these publications that users recognise and abide by the legal requirements associated with these rights.

### Take down policy

The University of Edinburgh has made every reasonable effort to ensure that Edinburgh Research Explorer content complies with UK legislation. If you believe that the public display of this file breaches copyright please contact [openaccess@ed.ac.uk](mailto:openaccess@ed.ac.uk) providing details, and we will remove access to the work immediately and investigate your claim.



## A coiled-coil affinity-based system for the controlled release of biofunctionalized gold nanoparticles from alginate hydrogels

Audrey Roth, Frederic Murschel, Pierre-Luc Latreille, Vincent A. Martinez, Benoît Liberelle, Xavier Banquy, and Gregory De Crescenzo

*Biomacromolecules*, **Just Accepted Manuscript** • DOI: 10.1021/acs.biomac.9b00137 • Publication Date (Web): 05 Apr 2019

Downloaded from <http://pubs.acs.org> on April 12, 2019

### Just Accepted

“Just Accepted” manuscripts have been peer-reviewed and accepted for publication. They are posted online prior to technical editing, formatting for publication and author proofing. The American Chemical Society provides “Just Accepted” as a service to the research community to expedite the dissemination of scientific material as soon as possible after acceptance. “Just Accepted” manuscripts appear in full in PDF format accompanied by an HTML abstract. “Just Accepted” manuscripts have been fully peer reviewed, but should not be considered the official version of record. They are citable by the Digital Object Identifier (DOI®). “Just Accepted” is an optional service offered to authors. Therefore, the “Just Accepted” Web site may not include all articles that will be published in the journal. After a manuscript is technically edited and formatted, it will be removed from the “Just Accepted” Web site and published as an ASAP article. Note that technical editing may introduce minor changes to the manuscript text and/or graphics which could affect content, and all legal disclaimers and ethical guidelines that apply to the journal pertain. ACS cannot be held responsible for errors or consequences arising from the use of information contained in these “Just Accepted” manuscripts.



1  
2  
3  
4  
5  
6  
7 A coiled-coil affinity-based system for the controlled  
8  
9  
10  
11 release of biofunctionalized gold nanoparticles from  
12  
13  
14  
15 alginate hydrogels  
16  
17  
18  
19

20 *Audrey Roth<sup>1</sup>, Frederic Murschel<sup>2</sup>, Pierre-Luc Latreille<sup>2</sup>, Vincent A. Martinez<sup>3</sup>, Benoît*

21 *Liberelle<sup>1</sup>, Xavier Banquy<sup>2\*</sup>, Gregory De Crescenzo<sup>1\*</sup>*

22  
23  
24  
25  
26  
27  
28  
29 <sup>1</sup>Department of Chemical engineering, Groupe de Recherche en Sciences et Technologies  
30 Biomédicales (GRSTB), Bio-P<sup>2</sup> Research Unit, École Polytechnique de Montréal, Montréal, QC,  
31  
32  
33  
34 Canada

35  
36  
37 <sup>2</sup>Canadian Research Chair in Bioinspired materials, Faculty of Pharmacy, Université de Montréal,  
38  
39  
40 Montréal, QC, Canada

41  
42 <sup>3</sup>School of Physics and Astronomy, The University of Edinburgh, Peter Guthrie Tait Road,  
43  
44  
45 Edinburgh, EH9 3FD, UK

1  
2  
3 ABSTRACT  
4  
5  
6

7 Affinity-based systems represent a promising solution to control the delivery of therapeutics using  
8 hydrogels. Here, we report a hybrid system that is based on the peptidic E/K coiled-coil affinity  
9 pair to mediate the release of gold nanoparticles from alginate scaffolds. On the one hand, the gold  
10 nanoparticles were functionalized with Ecoil-tagged epidermal growth factor (EGF). The  
11 bioactivity of the grafted EGF and the bioavailability of the Ecoil moiety were confirmed by EGF  
12 receptor phosphorylation assays and by capturing the functionalized nanoparticles on a Kcoil-  
13 derivatized surface, respectively. On the other hand, alginate chains were modified with azido-  
14 homoalanine Kcoil (Aha-Kcoil) by azide-alkyne click chemistry. The hybrid system was formed  
15 by dispersing NPs functionalized with Ecoil-tagged EGF in alginate hydrogels containing either  
16 0, 10 or 20% of Kcoil-modified alginate (Alg-Kcoil). With 20% of Alg-Kcoil, the release of Ecoil-  
17 functionalized NPs was reduced by half when compared to the release of NPs without Ecoil,  
18 whereas little to no differences were noticed with either 0 or 10% of Alg-Kcoil. Differential  
19 dynamic microscopy was used to determine the diffusion coefficient of the NPs, and the results  
20 showed a decrease in the diffusion coefficient of Ecoil-functionalized NPs, when compared to bare  
21 pegylated NPs. Altogether, our data demonstrated that the E/K coiled-coil system can control the  
22 release of NPs in a high Kcoil content alginate gel, opening diverse applications in drug delivery.  
23  
24  
25  
26  
27  
28  
29  
30  
31  
32  
33  
34  
35  
36  
37  
38  
39  
40  
41  
42  
43

44  
45  
46  
47  
48 KEYWORDS. Coiled-coil, affinity, diffusion, hydrogel, gold nanoparticle, differential dynamic  
49 microscopy  
50  
51  
52  
53  
54  
55  
56  
57  
58  
59  
60

## 1. Introduction

1  
2  
3  
4  
5  
6  
7  
8 Researchers from numerous fields strive to develop systems that allow for the controlled and  
9  
10 efficient delivery of therapeutics, especially for long-term release. A number of complementary  
11  
12 strategies have emerged in that endeavor; they have been applied to many types of therapeutics,  
13  
14 from hydrophobic molecules to nucleic acids, peptides and proteins. A very popular method  
15  
16 consists in encapsulating the therapeutic agent in polymeric micro- or nanoparticles.<sup>1,2</sup> Release is,  
17  
18 in this case, governed by particle degradation and passive diffusion of the therapeutic. The  
19  
20 encapsulation process however tends to degrade peptides and proteins and has therefore been  
21  
22 primarily applied to small hydrophobic molecules.<sup>3</sup> The incorporation of the drug in a polymeric  
23  
24 scaffold is another frequently encountered strategy, for which the release is mainly regulated by  
25  
26 scaffold swelling and/or scaffold degradation, be it in bulk or by surface erosion, although passive  
27  
28 diffusion can play a significant role.<sup>4</sup> Affinity-based delivery strategies have recently gained a lot  
29  
30 of interest as they may offer more versatility and can promote long-term and continuous release of  
31  
32 drugs or proteins.<sup>3</sup> Indeed, by incorporating a specific biological anchor in a polymeric scaffold,  
33  
34 the molecule diffusion can be dramatically slowed down and thus release can be stretched over a  
35  
36 long period of time.<sup>3,5</sup> These systems have been growing in number and variety, and show potential  
37  
38 for an increasing number of applications.<sup>6-10</sup>

39  
40  
41  
42  
43  
44  
45 Most affinity-based strategies thus far have relied on naturally occurring interactions between the  
46  
47 protein or drug of interest and one of its biological partners. Glycans such as heparin and sulfates  
48  
49 have been widely reported as a means to sequester heparin-binding proteins within scaffolds<sup>11</sup>,  
50  
51 which has significantly extended the duration of protein delivery up to several days.<sup>6,12</sup> Similarly,  
52  
53 complexes of  $\beta$ -cyclodextrins have been covalently incorporated in hydrogels to control the release  
54  
55  
56  
57  
58  
59  
60

1  
2  
3 of hydrophobic low molecular weight proteins.<sup>13</sup> Some research groups have engineered  
4 polysaccharide fragments and peptide sequences inspired by natural biomolecules to interact more  
5 specifically with the therapeutic of interest and/or to better control its delivery.<sup>14</sup> For instance, Lin  
6 *et al.* were able to control the release profile of a growth factor from a poly(ethylene glycol) (PEG)  
7 hydrogel by functionalizing PEG chains with affinity binding peptides.<sup>7</sup> Similarly, Wang *et al.*  
8 developed a competitive affinity-based system to release multiple proteins at different timepoints  
9 of the treatment.<sup>8</sup> More precisely, the vascular endothelial and the platelet-derived growth factors  
10 were immobilized on polystyrene microparticles using two different aptamers and then those  
11 microparticles were dispersed in a hydrogel. Protein release could then be triggered by simple  
12 incubation of a competitive aptamer sequence. Regardless, systems based on natural interactions  
13 suffer from a lack of versatility. Indeed, most designs only suit a narrow panel of therapeutic  
14 agents, given that each drug may require its own partner and specific hydrogel characteristics.  
15 Moreover, the release profiles are dictated by the thermodynamics of the interaction, which are  
16 hardly tunable for natural partners. The advances in biomolecule design and synthesis, notably by  
17 protein engineering, may offer a way to circumvent these issues and fulfill the current need for  
18 more flexibility and finer control of spatiotemporal delivery.

19  
20  
21  
22  
23  
24  
25  
26  
27  
28  
29  
30  
31  
32  
33  
34  
35  
36  
37  
38  
39  
40  
41 Coiled-coils are a ubiquitous motif found in proteins that has been discovered more than six  
42 decades ago and has been the core subject of many scientific works. The research based on *de*  
43 *novo* designed coiled-coil forming peptides has led to a robust knowledge of the determinants of  
44 their interactions.<sup>15-17</sup> The rational design of peptide sequences that feature tunable specificity,  
45 stability and oligomerization state has therefore been dramatically facilitated. It has been exploited  
46 for various tissue engineering and gene delivery applications,<sup>18</sup> and several proteins including  
47 growth factors, transcription factors and antibodies have been grafted onto polymer-based  
48  
49  
50  
51  
52  
53  
54  
55  
56  
57  
58  
59  
60

1  
2  
3 structures thanks to coiled-coil complexes.<sup>19–22</sup> Our group previously developed two de novo  
4 designed peptides, namely the Ecoil and the Kcoil, which design is based on the repetitions of  
5 seven distinct amino acids (a heptad). When mixed together, the peptides spontaneously form a  
6 coiled-coil heterodimeric complex, which affinity can be modulated by the number of heptads and  
7 their sequence, especially the aliphatic residues that comprise the hydrophobic core of the  
8 interaction.<sup>23–25</sup> The rationale of this research was to investigate the potential of coiled-coil  
9 interactions for the preparation of novel hybrid systems, that is, hydrogels that can deliver  
10 biofunctionalized nanoparticles (*e.g.* decorated on their surface with proteins or with encapsulated  
11 drugs), at a speed that is not only dependent on particle diffusion or gel degradation but that is  
12 tuned by specific affinity interactions.  
13  
14  
15  
16  
17  
18  
19  
20  
21  
22  
23  
24  
25

26  
27 To produce such system, we developed an Ecoil-decorated nanoparticle that can interact via  
28 specific coiled-coil interaction with Kcoil-grafted hydrogel. More precisely, we report, on the one  
29 hand, the functionalization of gold nanoparticles (AuNPs) with the Ecoil peptide as well as the  
30 human epidermal growth factor (EGF) using a cysteine-tagged Ecoil-EGF chimeric protein.  
31 AuNPs are interesting candidates for their biomedical applications in cancer (radiotherapy<sup>26</sup> and  
32 photothermal therapy<sup>27</sup>), imaging and drug delivery<sup>28</sup>. Their surface functionalization with  
33 therapeutics or peptides is well-documented.<sup>28</sup> On the other hand, we report a polymeric scaffold  
34 made from alginate chains that were covalently modified with the complementary Kcoil peptide  
35 and designed to specifically interact with decorated AuNPs. Alginate gels indeed feature an  
36 excellent biocompatibility, a wide use as injectable gels and unique gelation properties.<sup>29</sup> The  
37 AuNPs/hydrogel system was formed by simple coincubation of the Ecoil-bearing nanoparticles  
38 with the Kcoil-modified alginate chains during gelation. Affinity-based systems have been  
39 reported for protein release from hydrogels, while nanoparticles have been entrapped within gels  
40  
41  
42  
43  
44  
45  
46  
47  
48  
49  
50  
51  
52  
53  
54  
55  
56  
57  
58  
59  
60

1  
2  
3 for delayed delivery.<sup>5,30</sup> This is however the first report, to the best of our knowledge, that  
4 combines both strategies, that is, to sequester nanoparticles within a hydrogel and to release them  
5  
6 in a controlled fashion using a specific affinity interaction.<sup>3,31</sup>  
7  
8  
9

10 The characterization of the biofunctionalized nanoparticles was carried out by dynamic light  
11 scattering (DLS), transmission electron microscopy (TEM) and <sup>1</sup>H nuclear magnetic resonance  
12 (NMR) as well as enzyme-linked immunosorbent assays (ELISA) to assess the bioavailability of  
13 both the Ecoil and EGF moieties. The impact of Kcoil concentration in the hydrogel on the  
14  
15 diffusive properties of the AuNPs was then investigated using differential dynamic microscopy  
16 (DDM) and typical release tests. Both assays indicated that the formation of the Ecoil/Kcoil  
17 complex significantly hampered the movement of nanoparticles, and thus that this affinity-based  
18 strategy is suitable to prolong the release of NPs from hydrogels. The biological activity of the  
19 EGF moiety displayed on the NPs surfaces was also demonstrated by *in vitro* cellular assays, both  
20 prior and after their release from the hydrogels.  
21  
22  
23  
24  
25  
26  
27  
28  
29  
30  
31  
32  
33  
34  
35  
36  
37  
38  
39  
40  
41  
42  
43  
44  
45  
46  
47  
48  
49  
50  
51  
52  
53  
54  
55  
56  
57  
58  
59  
60



## 2. Experimental

### 2.1 Materials

Cysteine-tagged Ecoil-EGF (CEE) was produced in HEK 293-6E cells and purified by immobilized metal-ion affinity chromatography (IMAC) followed by size-exclusion chromatography, as previously described.<sup>32</sup> Protein concentration was determined by an enzyme-linked immunosorbent assay (ELISA) against EGF and analyzed by SDS-PAGE. Purified CEE was then stored at -80 °C until use. The azidohomoalanine-terminated Kcoil peptides (AhaGG(KVSALKE)<sub>5</sub>, or Aha-Kcoil) were synthesized by the peptide facility at University of Colorado (Denver, CO). Untagged recombinant human EGF and ELISA kit were purchased from R&D Systems (Minneapolis, MN). Sodium alginate ( $M_w = 171$  kDa) (IL-6G) were purchased from Kimica corporation (New-York, NY). Thiolated polyethylene glycol (PEG-SH) ( $M_w = 5$  kDa) was obtained from Jenkem Technology (Dallas, TX). MilliQ water was generated with a Millipore Gradient A10 purification system. Dulbecco's modified Eagle's medium (DMEM), fetal bovine serum (FBS) and gentamicin were obtained from Gibco (Burlington, VT). 75-cm<sup>2</sup> CellBIND flasks and 48- and 96-well CellBIND plates for cell cultures were purchased from Corning (Corning, NY). All other products and chemicals were purchased from Sigma-Aldrich Canada Ltd. (Oakville, ON), unless otherwise specified. Absorbance measurements were carried out on a Victor V Multilabel Counter from PerkinElmer Inc. (Woodbridge, ON) or using a Spark® multiplate reader from Tecan Group Ltd (Männedorf, Switzerland).

### 2.2 Biofunctionalization of gold nanoparticles

#### 2.2.1 Synthesis and characterization of gold nanoparticles

1  
2  
3 Gold nanoparticles (AuNPs) were synthesized using a citrate reduction method according to a  
4 previously published procedure.<sup>33</sup> Briefly, trisodium citrate (0.94 mL at 11.4 mg/mL) was rapidly  
5 injected in a boiling chloroauric solution (50 mL at 0.1 mg/mL in MQ water) under vigorous  
6 stirring and heating for 5 min, then cooled to room temperature (RT). The color of the solution  
7 changed from blue to deep red.  
8  
9

10  
11  
12 The NPs sizes were characterized by dynamic light scattering (DLS) using a Malvern Zetasizer  
13 (Malvern, UK) and by transmission electron microscopy (TEM, field emission 2100F, JEOL,  
14 Tokyo, Japan). The number of gold atoms per nanoparticle ( $N$ ) was estimated using<sup>34</sup>  
15  
16

$$17 \quad N = \frac{\pi \rho D^3}{6 M}, \quad (1)$$

18 where  $\rho$  is the density for face-centered cubic gold (19.3 g/cm<sup>3</sup>),  $M$  is the atomic weight of gold  
19 (197 g/mol) and  $D$  is the diameter of the NPs determined by TEM.  
20  
21

22 The final AuNPs concentration is given from  
23  
24

$$25 \quad [AuNPs] = \frac{m}{M \times N \times V}, \quad (2)$$

26 where  $m$  is the initial mass of gold and  $V$  is the final volume of the solution. In our experimental  
27 conditions, the concentration of the pristine gold nanoparticles was  $8.2 \times 10^{11}$  particles/mL or 1.4  
28 nM, and their diameter was  $18 \pm 2$  nm according to TEM. The stock solution was used to determine  
29 the AuNPs extinction coefficient at 531 nm, i.e.  $\epsilon_{AuNP} = 5.53 \times 10^8 \text{ M}^{-1} \cdot \text{cm}^{-1}$ , which is in good  
30 agreement with the literature for particles of this size.<sup>35</sup> After functionalization of the gold  
31 nanoparticles, the concentration of coated AuNPs was evaluated via UV-Vis measurements at 531  
32 nm.  
33  
34

### 35 2.2.2 PEGylation of gold nanoparticles

36  
37  
38  
39  
40  
41  
42  
43  
44  
45  
46  
47  
48  
49  
50  
51  
52  
53  
54  
55  
56  
57  
58  
59  
60

1  
2  
3 After synthesis, the AuNPs were stabilized by means of decoration with a low density of thiolated  
4 polyethylene glycol (PEG-SH) ( $M_w = 5$  kDa). The gold nanoparticles exposing a low density of  
5 PEG (NP-PEG<sub>LD</sub>) were obtained by injecting ca. 7  $\mu$ L of PEG-SH in 20 mL of the citrate solution  
6  
7  
8  
9 containing the AuNPs (final concentrations of 0.5  $\mu$ M PEG-SH and 1.4 nM AuNPs). After 16 h  
10  
11  
12 under stirring, the NP-PEG<sub>LD</sub> were centrifuged one time (10,000  $\times g$  for 30 min) and the  
13  
14 supernatant was discarded to remove unreacted PEG-SH.  
15  
16

17  
18 The amount of PEG-SH on the particles was determined using a  $^1\text{H}$  NMR-based method as  
19  
20 previously described.<sup>36</sup> Briefly, PEGylated NPs (700  $\mu$ L, 5.4 nM) were digested overnight with 7  
21  
22  $\mu$ L of Aqua Regia solution (37% HCl and 68-70% HNO<sub>3</sub> in a 3:1 ratio v/v). The resulting mixture  
23  
24 was then freeze-dried and resuspended in deuterium oxide (D<sub>2</sub>O) to reach a final volume of 700  
25  
26  $\mu$ L. Acetonitrile (ACN) was used as a standard to quantify the PEG-SH concentrations, i.e. 7  $\mu$ L  
27  
28 of 0.24% v/v ACN in water was added to each sample. The PEG-SH concentration was evaluated  
29  
30 by calculating the ratio between the integration of two peaks at specific positions for PEG-SH (3.7  
31  
32 ppm) and ACN (2.06 ppm). The PEG-SH concentration of each sample was determined using a  
33  
34 standard curve ranging from 0.1 to 200  $\mu$ M of PEG-SH.  
35  
36  
37  
38

### 39 2.2.3 Cys-Ecoil-EGF grafting on the pegylated gold nanoparticles

40

41  
42 The NP-PEG<sub>LD</sub> were coated with cysteine-tagged Ecoil-EGF (CEE) thanks to the thiol group  
43  
44 displayed by the cysteine. NP-PEG<sub>LD</sub> were mixed with CEE (final concentrations of 1.4 nM and  
45  
46 500 nM, respectively) in MQ water containing dextran chains that acted as a labware non-specific  
47  
48 adsorption blocker (10 mg/L of pristine dextran,  $M_w = 70$  kDa). The mixture was allowed to react  
49  
50 for 16 h under gentle agitation. To enhance NPs stability, PEG-SH was then added at a final  
51  
52 concentration of 50  $\mu$ M for 2 h to generate highly dense PEG-coated NPs (NP-PEG<sub>HD</sub>). Unreacted  
53  
54  
55  
56  
57  
58  
59  
60

1  
2  
3 material was removed by performing 4 centrifugations cycles ( $10,000 \times g$  for 30 min). For each  
4 cycle, 1.9 mL of supernatant were discarded and the remaining 100  $\mu\text{L}$  of CEE-coated  
5 nanoparticles (NP-CEE-PEG<sub>HD</sub>) were resuspended in 1.9 mL of phosphate buffered saline solution  
6 (PBS, 10 mM sodium phosphate and 150 mM of KCl/NaCl salts) supplemented with 0.1% v/v  
7 Tween-20 (PBS-T). As controls, NP-PEG<sub>LD</sub> were incubated with untagged EGF or without added  
8 EGF and were subjected to the same purification and blocking procedures. The resulting NPs were  
9 named NP-EGF-PEG<sub>HD</sub> and NP-PEG<sub>HD</sub>, respectively. The final amount of PEG-SH grafted on NP  
10 preparations was determined using the protocol described in the previous section.  
11  
12  
13  
14  
15  
16  
17  
18  
19  
20  
21

#### 22 2.2.4 EGF quantification

23  
24  
25 Effectiveness of the CEE grafting on the NPs surface was confirmed by a competitive enzyme-  
26 linked immunosorbent assay (ELISA) against EGF. Polystyrene 96-well plates were first saturated  
27 with the growth factor overnight (16 h) using 100  $\mu\text{L}$  of 5 nM Ecoil-EGF per well. The wells were  
28 then blocked with 50  $\mu\text{L}$  of 1% w/v BSA in PBS for 1 h. In parallel, the NP samples were mixed  
29 1:1 v/v with biotinylated anti-EGF antibodies (100 pM in PBS-T) for 1 h, while known EGF  
30 concentrations were mixed with antibodies for calibration. 50  $\mu\text{L}$  of the NPs/antibodies mixtures  
31 were then incubated in the EGF pre-coated wells for 1 h. Detection was performed by adding 50  
32  $\mu\text{L}$  of horseradish peroxidase (HRP)-streptavidine conjugate for 20 min followed by a revelation  
33 step using 50  $\mu\text{L}$  of substrate solution. A rinsing step was performed after each incubation (3  
34 rinsing cycles with 150  $\mu\text{L}$  of PBS-T). Absorbance was read at 630 nm and 531 nm for correction.  
35  
36  
37  
38  
39  
40  
41  
42  
43  
44  
45  
46  
47  
48

#### 49 2.3 Bioadhesion of the functionalized nanoparticles

50  
51  
52 The ability of the Ecoil moiety exposed on the NP-CEE-PEG<sub>HD</sub> surface to interact with its binding  
53 partner, the Kcoil, was assessed by immobilizing functionalized NPs on a Kcoil-coated surface.  
54  
55  
56  
57  
58  
59  
60

1  
2  
3 Kcoil-bearing dextran surfaces were prepared in 96-well plates as previously described.<sup>22</sup>  
4  
5 Functionalized wells were first blocked with BSA (1% w/v in PBS, 100  $\mu$ L/wells) for 1 h. The  
6  
7 NP-CEE-PEG<sub>HD</sub>, NP-EGF-PEG<sub>HD</sub> and NP-PEG<sub>HD</sub> were then injected at a concentration of 140  
8  
9 pM of particles for 1 h. The immobilized NPs were detected using an ELISA against EGF, thanks  
10  
11 to a protocol adapted from a previously reported work.<sup>37</sup> Briefly, 50  $\mu$ L of biotinylated anti-EGF  
12  
13 antibodies were added during 30 min. Detection and rinsing steps were carried out as described in  
14  
15 the previous section.  
16  
17  
18  
19

## 20 2.4 Kcoil grafting on alginate

21  
22

23 Kcoil peptides were covalently grafted on alginate via an alkyne-azide click chemistry. Sodium  
24  
25 alginate (1.5 g) was first dissolved in 10 mL of 0.5 M NaOH. 6.5 mL of undiluted glycidyl  
26  
27 propargyl ether (GPE, 90+% purity) was added and the mixture was allowed to react at RT under  
28  
29 agitation for 24 h. The product was then dialyzed (cut-off of 8 kDa) against MQ water for 72 h,  
30  
31 freeze-dried and stored at 4 °C until use.  
32  
33  
34

35 The azide-terminated Kcoil (Aha-Kcoil) was then grafted on the GPE-modified alginate (Alg-  
36  
37 GPE). 100 mg of Alg-GPE were dissolved in 10 mL of MQ water with final concentrations of 1  
38  
39 mM of Tris(3-hydroxypropyltriazolymethyl)amine (THPTA), 2.5 mM of copper sulfate (CuSO<sub>4</sub>)  
40  
41 and 5 mM of sodium ascorbate. Aha-Kcoil was added at an azide:alkyne ratio of 1:40. The mixture  
42  
43 was then allowed to react at RT for 48 h under agitation and in the dark. Note that after 24 h of  
44  
45 reaction time, 500  $\mu$ L of 100 mM sodium ascorbate in MQ water was added in the mixture. Two  
46  
47 ultrafiltration cycles in a 100 mM EDTA solution followed by three cycles with MQ water were  
48  
49 carried out using Amicon centrifugal filter (cut-off of 5 kDa). The polymer was then freeze-dried  
50  
51 and stored at 4 °C until use.  
52  
53  
54  
55  
56  
57  
58  
59  
60

1  
2  
3 The amount of grafted Kcoil per alginate chain was evaluated by a 2,4,6-Trinitrobenzenesulfonic  
4 acid solution (TNBS) assay which allows a quantification of the amines on the peptides. The assay  
5 protocol was adapted from previous work.<sup>38,39</sup> Briefly, alginate-Kcoil was diluted at 4 mg/mL in  
6 sodium bicarbonate (100 mM, pH 8.5). 100  $\mu$ L of the solution was mixed with 50  $\mu$ L of TNBS  
7 (0.01% w/v in sodium bicarbonate, 100 mM, pH 8.5) in a 96-well plate. After 2 h at 37°C, 50  $\mu$ L  
8 of sodium dodecyl sulfate (10% w/v in MQ water) and 25  $\mu$ L of MQ water were added to each  
9 well. The absorbance was read at 340 nm and 630 nm for reference. A calibration curve was plotted  
10 using known concentration of glycine (range between 4 and 125  $\mu$ M) and the molar extinction  
11 coefficient was corrected by the one for the amine of the lysine side-chain ( $\epsilon_{\text{glycine}}=13400 \text{ M}^{-1} \cdot \text{cm}^{-1}$   
12 <sup>38</sup> and  $\epsilon_{\text{lysine}}=12000 \text{ M}^{-1} \cdot \text{cm}^{-1}$ ).

## 27 2.5 NP Release from the alginate matrix

30 For the NPs release studies, NPs solutions in PBS were mixed with alginate in a 1:1 ratio. More  
31 precisely, 8.1 nM of NP-CEE-PEG<sub>HD</sub> and NP-PEG<sub>HD</sub> were mixed with solutions containing 80-  
32 90% w/w of unmodified alginate plus 10% w/w of GPE-modified, 10% w/w of Kcoil-modified or  
33 20% w/w of Kcoil-modified alginate (resp. Alg-Kcoil0%, Alg-Kcoil10% and Alg-Kcoil20%) for  
34 a total of 2% w/v of alginate in water. 50  $\mu$ L of the mixture (alginate and NPs) were poured in a  
35 96-well plate and gels were formed by adding 50  $\mu$ L of CaCl<sub>2</sub> (0.1 M in water) for 1 h. CaCl<sub>2</sub> was  
36 then removed and gels were incubated in 200  $\mu$ L of PBS at RT and under mild agitation (20 RPM).  
37 At each timepoint (0, 2, 4, 6, 9, 24 and 72 h), gels were removed from the wells and dissolved with  
38 20  $\mu$ L of sodium citrate (350  $\mu$ M). Final volumes were adjusted to 110  $\mu$ L and the concentration  
39 of NPs within the samples was determined by absorbance at 531 nm.

## 54 2.6 Differential dynamic microscopy (DDM)

1  
2  
3 NP-CEE-PEG<sub>HD</sub> and NP-PEG<sub>HD</sub> were mixed with Alg-Kcoil10%, Alg-Kcoil20% or MQ water in  
4 an equal volume (final concentration of 8.1 nM of nanoparticles and 1% w/v of alginate). 180  $\mu$ L  
5 of the mixtures were injected in 0.4-mm thick glass capillaries (Vitrocom, Canada). Capillaries  
6 containing alginate were opened on both ends and incubated in a CaCl<sub>2</sub> solution (20 mM) for 24 h  
7 for complete gelation to occur. All capillaries were sealed using petroleum jelly prior to DDM  
8 experiments.<sup>40</sup> DDM is a correlation-based microscopy technique that enables the characterisation  
9 of particle dynamics in complex systems.<sup>41–43</sup> Full details about DDM analysis can be found  
10 elsewhere<sup>44–46</sup> and only an overview is presented below.

11  
12 Videos were recorded at 100 frames per second for 41 seconds using an upright bright-field  
13 microscope (Olympus BX81) equipped with a high acquisition-speed camera (Hamamatsu Orca-  
14 Flash 4.0 V3) and a 20X magnification phase contrast objective (Olympus Plan Ph1, NA = 0.4).  
15 From those movies, power spectrums of the difference between all pairs of images (separated by  
16 the same delay time  $\tau$ ) were calculated and averaged yielding the averaged Differential Image  
17 Correlation Function  $g(\vec{q}, \tau)$ . For isotropic motion the azimuthal average was calculated, giving  $g$   
18  $(q, \tau) = \langle g(\vec{q}, \tau) \rangle_{\vec{q}}$  with  $q$  being the spatial frequency, which under appropriate imaging  
19 conditions<sup>44–46</sup> is related to the intermediate scattering function  $f(q, \tau)$  probing for particle  
20 dynamics so that:

$$21 \quad g(q, \tau) = A(q)(1 - f(q, \tau)) + B(q), \quad (3)$$

22 where  $A(q)$  is the amplitude signal and  $B(q)$  the background noise. Fitting  $g(q, \tau)$  with appropriate  
23 models of  $f(q, \tau)$  can access particle dynamics. We used a generalized exponential:

$$24 \quad f(q, \tau) = e^{-\left(\frac{\tau}{\tau_R}\right)^\beta} \quad (4)$$

1  
2  
3 where  $\tau_R$  is the relaxation time and  $\beta$  is an exponent that provides insight about size polydispersity  
4 of particles and their interactions. For monodisperse non-interacting spheres in water,  $\beta = 1$  and  
5 the relaxation time is  $\tau_R = \frac{1}{q^2 D}$ , with  $D$  being the diffusion coefficient from which the particle  
6 radius,  $r$ , can be extracted following the Stoke-Einstein equation:  
7  
8  
9  
10  
11  
12

$$D = \frac{kT}{6\pi nr} \quad (5)$$

13  
14  
15  
16  
17

18 with  $kT$  the thermal energy and  $n$  the viscosity.  $\beta < 1$  usually indicates size polydispersity and/or  
19 interactions, be it particle/particle or particle/gel interactions. We found that  $\beta$  was between 0.9  
20 and 1 both in water and in the alginate gels, suggesting that interactions were negligible. We  
21 verified that the relaxation times  $\tau_R$  were proportional to  $q^{-2}$ , therefore an effective diffusion  
22 coefficient  $D$  could be extracted from  $\tau_R = q^{-2} D^{-1}$ .  
23  
24  
25  
26  
27  
28  
29

## 30 2.7 In vitro cell assay

31  
32  
33

### 34 2.7.1 Cell culture

35  
36  
37

38 A431 cells overexpressing the EGF receptor were maintained in 75-cm<sup>2</sup> flasks using Dulbecco's  
39 modified Eagle's medium (DMEM) supplemented with 10% v/v of fetal bovine serum (FBS) and  
40 0.1% v/v of penicillin-streptomycin. The flasks were kept in a humidified incubator (37 °C, 5%  
41 CO<sub>2</sub>) until 85-90% confluence.  
42  
43  
44  
45  
46  
47

### 48 2.7.2 Phosphorylation assay by Western Blot

49  
50

51 A431 cells were distributed in 48-well plates at a concentration of 0.6 10<sup>6</sup> cells/mL (0.5 mL per  
52 well). 20 h later, 85-90% of confluence was reached and each well was rinsed 2 times with 1 mL  
53 of PBS. Cells were then starved for 3 h using 500  $\mu$ L of basal medium (DMEM with no serum).  
54  
55  
56  
57  
58  
59  
60



1  
2  
3 The basal medium was removed from each well and the cells were exposed during 5 min to 50  $\mu$ L  
4 of the functionalized NPs (at an equivalent EGF concentration of 1.5 nM, according to ELISA) or  
5 to 50  $\mu$ L of soluble EGF (EGF concentrations of 0.1, 1 and 10 nM). The wells were washed twice  
6  
7 with 1 mL of PBS supplemented with 1 mM of sodium-orthovanadate, and the cells were then  
8  
9 lysed using 75  $\mu$ L of a commercial lysis buffer supplemented with 0.1 mM of sodium-  
10  
11 orthovanadate. Insoluble materials were removed by centrifugation (10,000  $\times$  g, 20 min, 4  $^{\circ}$ C).  
12  
13 Samples were then analysed for phosphotyrosine levels by Western Blot, using mouse PY99  
14  
15 (Santa Cruz, CA) and anti-mouse-HRP antibodies, according to a previously-reported procedure.<sup>47</sup>  
16  
17 A Bradford assay was performed prior to gel electrophoresis to ensure that the same amount of  
18  
19 protein was loaded in each well. A ChemiDoc system (Biorad, Hercules, CA) and the ImageLab  
20  
21 software were used to image the nitrocellulose membrane and to analyse images, respectively.  
22  
23 Quantification of the level of phosphorylation in each well was enabled by the *Quantity tools* of  
24  
25 the software, using the signal obtained with soluble EGF (10, 1 and 0.1 nM) as a calibration.  
26  
27  
28  
29  
30  
31  
32  
33  
34  
35  
36  
37  
38  
39  
40  
41  
42  
43  
44  
45  
46  
47  
48  
49  
50  
51  
52  
53  
54  
55  
56  
57  
58  
59  
60

### 3. Results and discussion

We here report the engineering of an affinity-based system for the controlled release of biofunctionalized NPs from a hydrogel, using the high-affinity E/K coiled-coil interactions. This strategy makes use of AuNPs decorated with cysteine-tagged Ecoil-EGF (CEE) and of Kcoil-derivatized alginate hydrogels. AuNPs were stabilized through PEGylation, both before and after CEE functionalization (Figure 1.A), while the Kcoil peptide was grafted on the alginate chains using GPE-mediated alkyne:azide click chemistry (Figure 1.B). We here investigated the diffusive properties of the Ecoil-NPs as a function of Kcoil density in alginate hydrogels (Figure 1.C).

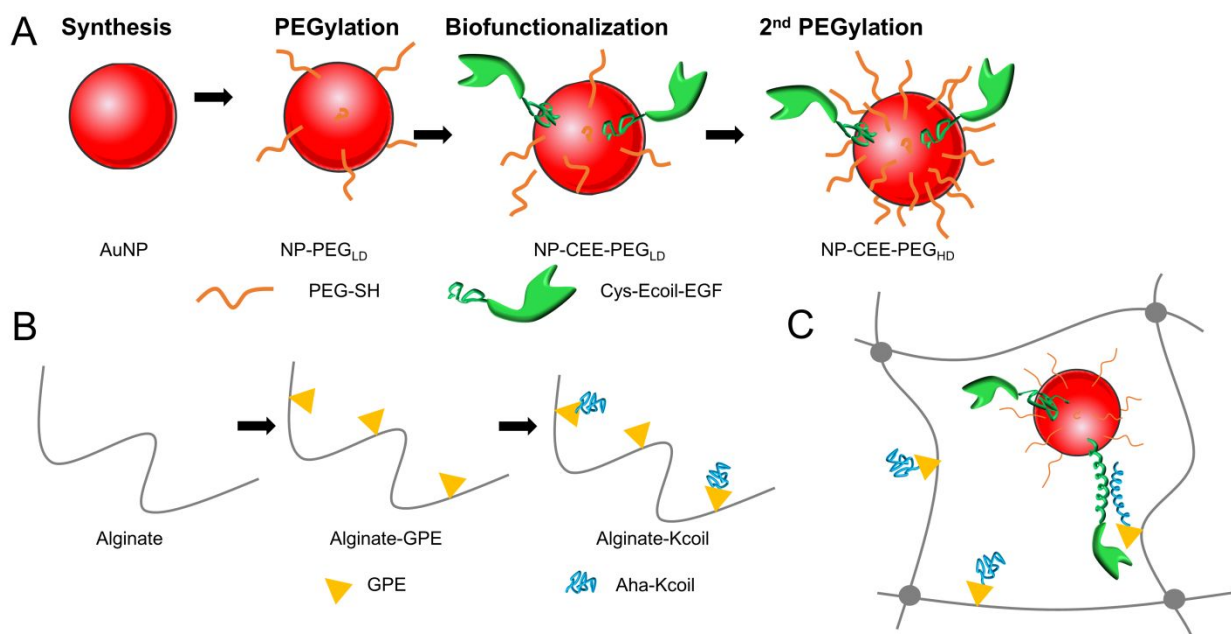


**Figure 1. Preparation of the affinity-based hybrid system using gold nanoparticles and an alginate scaffold.** (A) AuNPs were first PEGylated to a low level for stabilization. Cys-Ecoil-EGF (CEE) was then grafted via thiol-gold chemistry. A second PEGylation step was then performed for higher stability. (B) Alginate chains were first derivatized with an alkyne moiety using glycidyl propargyl ether (GPE). Azidohomoalanine-tagged Kcoil peptides (Aha-Kcoil) were then grafted via azide-alkyne click chemistry. (C) The dispersion of Ecoil-AuNPs in the Kcoil-alginate hydrogel enabled the formation of the E/K coiled-coil complex to slow down NPs release.

### 3.1 Characterization of pristine and functionalized NPs

Pristine and functionalized gold nanoparticles (AuNPs) were characterized using transmission electron microscopy (TEM) to determine NPs core diameter, dynamic light scattering (DLS) and differential dynamic microscopy (DDM) for hydrodynamic diameter,  $^1\text{H}$  nuclear magnetic resonance (NMR) for PEG density, enzyme-linked immunosorbent assays for EGF density and UV-Vis spectroscopy. The data are shown in Table 1 and Figure 2.

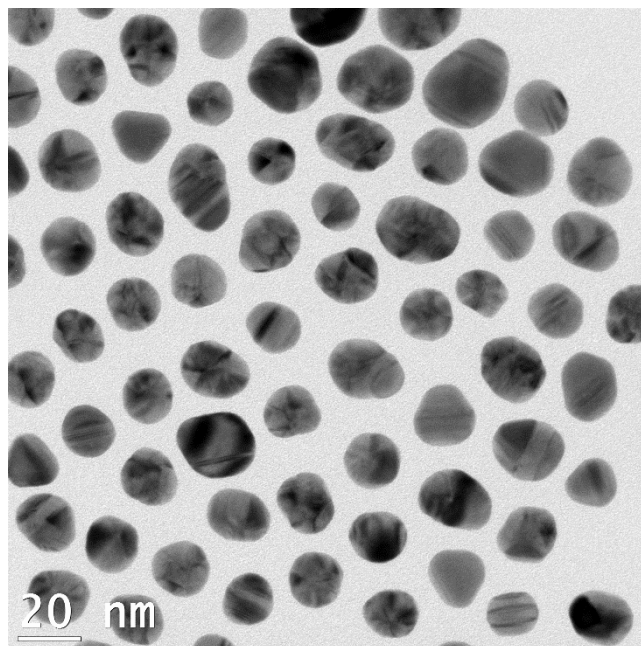


**Figure 2 : Transmission electron microscopy (TEM) image of AuNPs.**  
The average NPs diameter measured was  $18 \pm 2$  nm ( $n=100$ ).

DLS analysis indicated that the average hydrodynamic diameter of the synthesized AuNPs was  $d_h$ ,  $d_{LS} = 28 \pm 0$  nm with a polydispersity index of  $PDI = 0.29 \pm 0.00$ . Throughout the functionalization process (PEG then CEE then PEG again), the PDI of each NPs type did not significantly change ( $PDI = 0.29 \pm 0.01$ ,  $0.31 \pm 0.02$  and  $0.29 \pm 0.00$  for NP-CEE-PEG<sub>HD</sub>, NP-EGF-PEG<sub>HD</sub> and NP-

1  
2  
3 PEG<sub>HD</sub> respectively). The hydrodynamic diameter of NP-PEG<sub>LD</sub> was  $d_{h, DLS} = 55 \pm 3$  nm, that is,  
4  
5 the first PEGylation step induced an increase in diameter of 27 nm, which is in good agreement  
6  
7 with the literature.<sup>48</sup> After CEE grafting and a second PEGylation step, the NPs size further  
8  
9 increased to reach  $d_{h, DLS} = 62 \pm 2$  nm. The increase in size (7 nm) between NP-PEG<sub>LD</sub> and NP-  
10  
11 CEE-PEG<sub>HD</sub> indicated that the first low-density PEG layer allowed for both stabilization and  
12  
13 subsequent functionalization. NPs sizes were also determined by DDM. The diffusion coefficient  
14  
15 of each type of NPs was first measured in water. NPs sizes were calculated using the Stokes-  
16  
17 Einstein equation (Eq. 5) from the measured NPs diffusion coefficient  $D$ . The sizes of NP-CEE-  
18  
19 PEG<sub>HD</sub> and NP-PEG<sub>HD</sub> obtained using DDM were close to the values previously determined with  
20  
21 DLS (cf. Table 1), while the gap between both techniques can be attributed to a different analysis  
22  
23 of the intermediate scattering function (ISF) to take into account polydispersity effects.<sup>44,49</sup> For the  
24  
25 NP-PEG<sub>LD</sub>, the average number of PEG chain per NP was calculated at  $\sigma_{PEG} = 0.2 \pm 0.1$  thousands  
26  
27 of PEG chains. Of interest, NP-PEG<sub>HD</sub> particles had an average number of PEG per NP of  $\sigma_{PEG} =$   
28  
29  $2.6 \pm 0.8$  whereas NP-CEE-PEG<sub>HD</sub> and NP-EGF-PEG<sub>HD</sub> featured dramatically less PEG chains  
30  
31 per particle ( $\sigma_{PEG} = 0.8 \pm 0.3$  and  $\sigma_{PEG} = 0.5 \pm 0.0$ , respectively), which suggested that the grafting  
32  
33 of the protein on the NP surface hampered the grafting of PEG chains during the second  
34  
35 PEGylation step.  
36  
37  
38  
39  
40  
41  
42

43 The impact of the different functionalization on the NPs physical characteristics was also assessed  
44  
45 by UV-vis spectroscopy. A significant 4-nm increase in the maximum absorbance wavelength  $\lambda_{max}$   
46  
47 was observed between the NP-PEG<sub>LD</sub> and the fully functionalized NPs. A competitive ELISA was  
48  
49 developed to determine the average number of EGF protein per NP (corresponding to the EGF  
50  
51 concentration divided by the NPs concentration). The EGF density,  $\sigma_{EGF}$ , was found to be null ( $0.0$   
52  
53  $\pm 0.0$ ) for the pegylated NP-PEG<sub>HD</sub>, whereas  $\sigma_{EGF}$  reached  $1.0 \pm 0.6$  for NP-CEE-PEG<sub>HD</sub>.  
54  
55  
56  
57  
58  
59  
60

1  
2  
3 Interestingly, a similar density of  $\sigma_{\text{EGF}} = 1.2 \pm 0.0$  protein per particle was also obtained for NPs  
4 that were incubated with untagged EGF (NP-EGF-PEG<sub>HD</sub>). For this sample, the link between  
5 untagged EGF and the NP-PEG<sub>LD</sub> could be attributed to the EGF disulfide bonds interacting with  
6 the gold surface, as previously proposed by Song *et al.*<sup>50</sup>  
7  
8  
9  
10  
11  
12

13 **Table 1** : Characteristics of bare and functionalized gold nanoparticles.  
14  
15

	<b>AuNP</b>	<b>NP-PEG<sub>LD</sub></b>	<b>NP-CEE-PEG<sub>HD</sub></b>	<b>NP-EGF-PEG<sub>HD</sub></b>	<b>NP-PEG<sub>HD</sub></b>
$\lambda_{\text{max}}$ (nm) <sup>a</sup>	524	524	528	528	528
$d_{h, \text{DLS}}$ (nm) <sup>b</sup>	28 ± 0	55 ± 3	62 ± 2	64 ± 2	59 ± 2
<b>PDI</b> <sup>c</sup>	0.29 ± 0.00	0.28 ± 0.00	0.29 ± 0.01	0.31 ± 0.02	0.29 ± 0.00
$d_{h, \text{DDM}}$ (nm) <sup>d</sup>	-	-	53 ± 2	-	47 ± 0
$\sigma_{\text{PEG}}$ ( $\times 10^3$ ) <sup>e</sup>	-	0.2 ± 0.1	0.8 ± 0.3	0.5 ± 0.0	2.6 ± 0.8
$\sigma_{\text{EGF}}$ <sup>f</sup>	-	-	1.0 ± 0.6	1.2 ± 0.0	0.0 ± 0.0

16  
17  
18  
19  
20  
21  
22  
23  
24  
25  
26  
27  
28  
29  
30 <sup>a</sup> Peak absorbance wavelength

31 <sup>b</sup> Hydrodynamic diameter determined by DLS (Intensity distribution, mean ± SD, n = 3)

32 <sup>c</sup> Polydispersity index determined by DLS (Mean ± SD, n = 3)

33 <sup>d</sup> Hydrodynamic diameter determined by DDM (Mean ± SD, n = 5)

34 <sup>e</sup> Number of PEG chains per NP (Mean ± SD, n = 3)

35 <sup>f</sup> Number of EGF per NP (Mean ± SD, n = 3)  
36  
37  
38  
39  
40  
41  
42  
43  
44  
45

## 46 3.2 Bioadhesion and bioactivity of the functionalized AuNPs

47  
48  
49 The ability of the Ecoil moiety present at the NP-CEE-PEG<sub>HD</sub> surface to interact with its biological  
50 partner, the Kcoil peptide, was assessed by incubating the functionalized NPs on Kcoil-decorated  
51 multiwell plates. After incubation, the immobilized NP-CEE-PEG<sub>HD</sub> were detected using an HRP-  
52  
53  
54  
55  
56  
57  
58  
59  
60

1  
2  
3 labelled anti-EGF antibody. The ELISA data showed a significantly higher signal for NP-CEE-  
4 PEG<sub>HD</sub>, when compared to NP-EGF-PEG<sub>HD</sub> and NP-PEG<sub>HD</sub> for which no signal above the noise  
5  
6 level was detected (Figure 3.A). The results thus confirmed that a) the Ecoil tag was necessary for  
7  
8 NP capture on Kcoil-decorated surfaces and that b) the Ecoil moiety was bioavailable, i.e. both  
9  
10 accessible and functional, on the NP-CEE-PEG<sub>HD</sub>.  
11  
12  
13  
14

15 As for the EGF moiety on the NP-CEE-PEG<sub>HD</sub> surface, its biological activity was evaluated by the  
16  
17 ability of the growth factor to bind to its cognate receptor (EGFR) and induce EGFR  
18  
19 phosphorylation. For that purpose, A431 cells were selected as they are known to express high  
20  
21 levels of EGFR.<sup>51</sup> The cells were amplified in DMEM containing 10% v/v FBS until 80-90 %  
22  
23 confluence. After a 3 h period of starvation in serum-free medium, the cells were stimulated with  
24  
25 either soluble EGF (0 to 10 nM) or functionalized NPs (apparent EGF concentration of 1.5 nM  
26  
27 according to ELISA results). The cells were then lysed, cell debris were removed by centrifugation  
28  
29 and the amount of phosphorylated EGFR was quantified by Western Blot using an  
30  
31 antiphosphotyrosine antibody. The EGFR phosphorylation levels were compared to control  
32  
33 soluble EGF at concentrations ranging between 0 to 10 nM. Results show (Figure 3.B) that NP-  
34  
35 CEE-PEG<sub>HD</sub> and NP-EGF-PEG<sub>HD</sub> were able to induce a higher level of EGFR phosphorylation  
36  
37 when compared to soluble EGF. More precisely, when the NP-CEE-PEG<sub>HD</sub> and NP-EGF-PEG<sub>HD</sub>  
38  
39 particles were diluted to obtain a 1.5 nM concentration of EGF (as determined by ELISA), the  
40  
41 phosphorylation levels, that is, the degree of cell stimulation, were close to those obtained with a  
42  
43 soluble EGF concentration of  $5 \pm 2$  nM and  $13 \pm 2$  nM, respectively. Of interest, no signal was  
44  
45 obtained with NP-PEG<sub>HD</sub> particles, which confirmed that EGF-free NPs did not induce EGFR  
46  
47 phosphorylation. The apparently higher biological activity of the NP-tethered EGF could be the  
48  
49 result of the high proximity of the growth factors on the surface of the particles. Indeed, two  
50  
51  
52  
53  
54  
55  
56  
57  
58  
59  
60

1  
2  
3 proximate EGF are known to promote EGFR dimerization and increase the phosphorylation level  
4  
5 compared to their isolated counterparts.<sup>52</sup>  
6  
7

8  
9 As for the difference between NP-CEE-PEG<sub>HD</sub> and NP-EGF-PEG<sub>HD</sub>, it was previously shown that  
10  
11 the addition of a Cys-Ecoil N-terminal tag to EGF did not alter the biological activity of the protein  
12  
13 in solution.<sup>32</sup> The noticeable difference in EGFR phosphorylation levels obtained with the particles  
14  
15 decorated with EGF and CEE could thus be attributed to a higher bioavailability (for instance a  
16  
17 better orientation of the EGFR binding site) of EGF on the NP surface, when compared to CEE.  
18  
19 The other possible explanation is that the Ecoil, in its random conformation, interacts with EGF  
20  
21 binding site decreasing its affinity to its receptor.  
22  
23  
24

25  
26 Altogether, the phosphorylation assay demonstrated that both cysteine-Ecoil-tagged EGF and  
27  
28 untagged EGF grafted on NP-PEG<sub>LD</sub> were bioactive, and that their immobilization on NP surface  
29  
30 did enhance their biological activity. Nonetheless, since our goal is to control the release of NPs  
31  
32 via the Ecoil/Kcoil interaction, NP-CEE-PEG<sub>HD</sub> were selected for further characterization given  
33  
34 that NP-EGF-PEG<sub>HD</sub> could not interact with Kcoil-modified surfaces (cf. Figure 3.A).  
35  
36  
37  
38  
39  
40  
41  
42  
43  
44  
45  
46  
47  
48  
49  
50  
51  
52  
53  
54  
55  
56  
57  
58  
59  
60

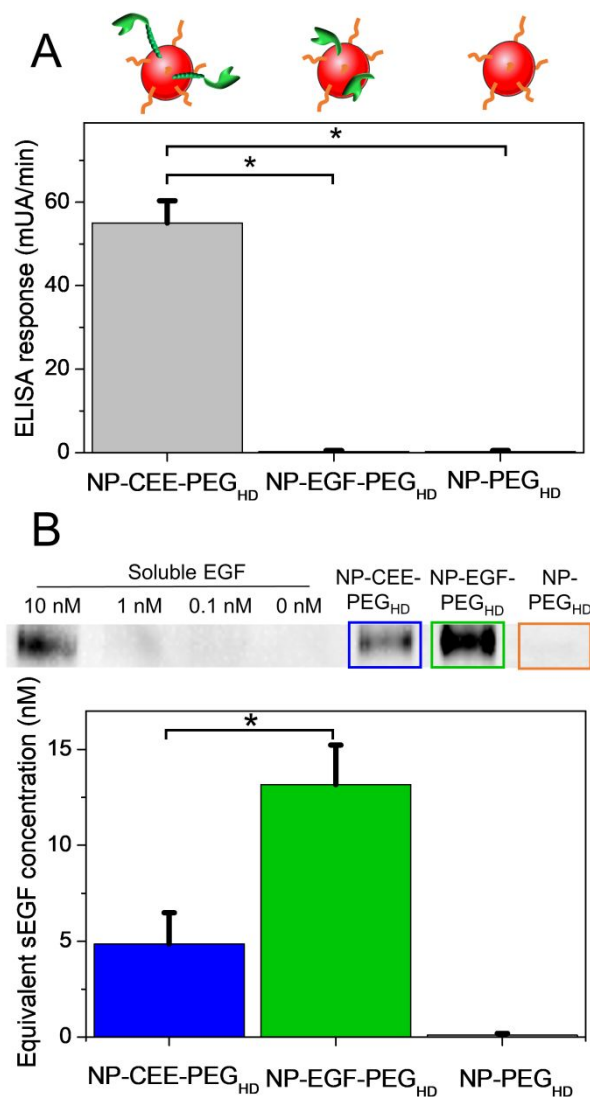


**Figure 3. Bioadhesion and bioactivity of functionalized NPs.**

(A) Bioadhesion on a Kcoil-derivatized surface of NP-CEE-PEG<sub>HD</sub>, NP-EGF-PEG<sub>HD</sub>, and NP-PEG<sub>HD</sub> as control, as detected by anti-EGF ELISA (n=3) (B) EGFR phosphorylation in A431 cells upon binding with soluble EGF (10, 1, 0.1 and 0 nM), NP-CEE-PEG<sub>HD</sub> or NP-EGF-PEG<sub>HD</sub> (EGF concentration of 1.5 nM according to ELISA) and NP-PEG<sub>HD</sub>, as monitored by Western Blot. The 180-kDa band immunoreactive to anti-phosphotyrosine antibodies (corresponding to EGFR) was quantified using a ChemiDoc and Image Lab software. Y-axis represents the equivalent concentration in soluble EGF (sEGF) (n = 3 for NP-CEE-PEG<sub>HD</sub> and NP-EGF-PEG<sub>HD</sub> and n = 1 for NP-PEG<sub>HD</sub>, \* indicates statistical differences between datasets (bilateral t-test, p < 0.05).



### 3.3 Characterization of Kcoil grafting on alginate

Kcoil peptides were grafted on the alginate chains using a two-step method, as illustrated in Figure 4. First, alkyne moieties were conjugated to alginate chain using glycidyl propargyl ether (GPE). L-azidohomoalanine (Aha)-terminated Kcoil was then covalently grafted to the polymer using alkyne-azide click chemistry.<sup>53</sup> In the present experimental conditions, the molar ratio was set to 1 Aha-Kcoil for 40 alkyne groups.

The alkyne ratio per chain was first quantified by <sup>1</sup>H NMR (Figure 4). A peak distinctly appeared at 3.4 ppm (peak A) after the alginate/GPE reaction and was attributed to the proton of the alkyne group. Using the peaks at 5.1 and 5.5 ppm as references (peaks M1 and G1, respectively, that were attributed to protons held by each alginate monomer),<sup>54</sup> we calculated that 29% of the alginate monomers were modified with an alkyne group.

As for the subsequent Kcoil grafting step, the amount of peptide per alginate monomer was evaluated thanks to the TNBS-based amine quantification test. Knowing that 1 Kcoil peptide holds 10 primary amine groups, the TNBS assay revealed that 77 % of the peptides in the alginate-GPE/Aha-Kcoil mixture reacted with alkyne groups. The yield of this click reaction is in good agreement with previous reports that used Aha and alkyne reactive groups.<sup>53,55,56</sup> Altogether, the 171-kDa alginate chains hold an average of 5 Kcoil peptides distributed among the 940 monomers.

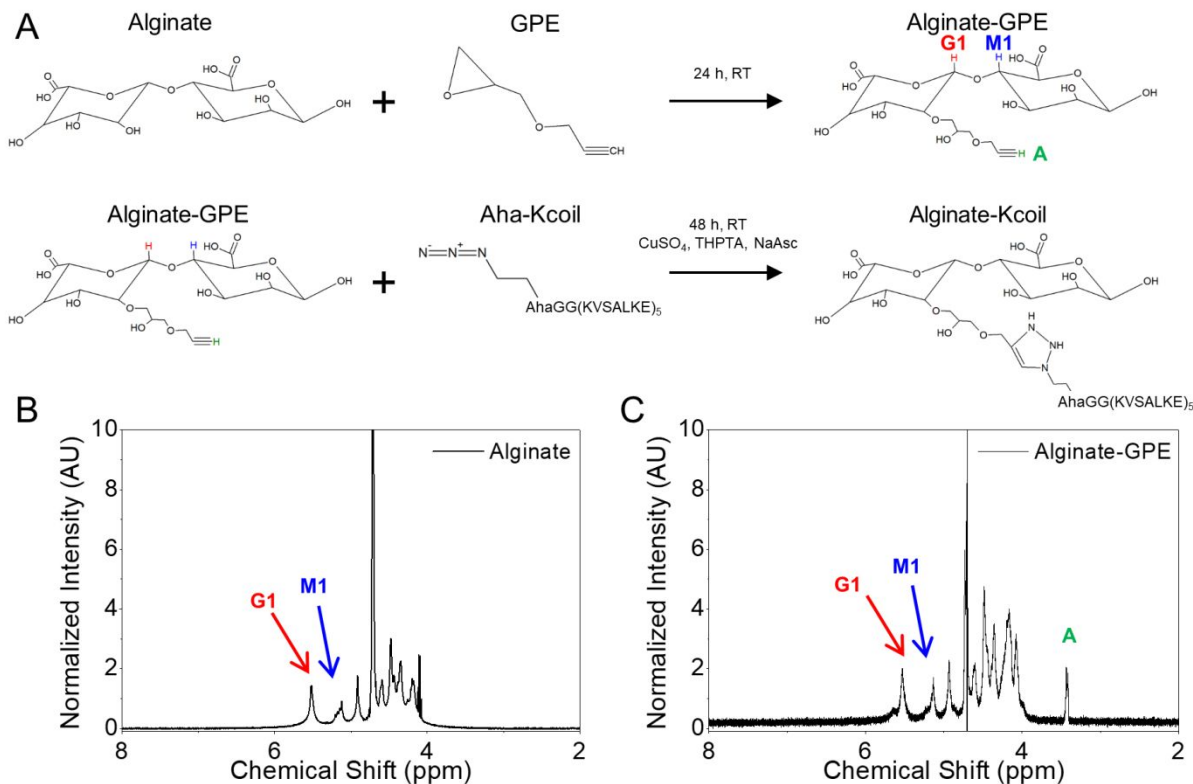


**Figure 4. Synthesis and characterization of Kcoil-derivatized alginate.**

(A) Alginate was first modified with glycidyl propargyl ether (GPE). Azide-terminated Kcoil peptides were then grafted on alginate-GPE via alkyne-azide click chemistry in presence of copper sulfate. (B and C) The percentage of alkyne-modified monomers was quantified by <sup>1</sup>H NMR using the peak at 3.4 ppm (peak A), corresponding to the alkyne, and the peaks at 5.5 ppm (G1) and 5.1 ppm (M1) as reference, corresponding to the total amount of monomers.

### 3.4 Diffusion and release tests

#### 3.4.1 Diffusion of the functionalized NPs

The diffusion of functionalized and pegylated NPs in alginate gels was investigated by DDM. Solutions of 2% w/v alginate containing either 10% or 20% w/w of Kcoil-modified alginate were mixed in a 1:1 (v/v) ratio with 16.3 pM of either NP-CEE-PEG<sub>HD</sub> or NP-PEG<sub>HD</sub>. The mixtures were injected in capillaries opened on both ends and were then immersed in a solution of 20 mM CaCl<sub>2</sub>, which initiated the gelation by diffusion of Ca<sup>2+</sup> ions. After 24 h, videos were taken at 100

1  
2  
3 fps for 41 s and the results are shown in Figure 5. Intermediate scattering functions (ISFs)  $f(q, \tau)$   
4  
5 were extracted from the autocorrelation function as described above. In the case of Alg-Kcoil10%,  
6  
7 a second slower dynamic process was observed, that was presumably due to a slow gel drift or the  
8  
9 presence of a few aggregates as observed from the recorded videos. For such cases, we used a  
10  
11 double generalised exponential model (from equations 3 and 4) for the ISFs when fitting the DICF  
12  
13  
14  
15  $g(q, \tau)$ :

$$16 \quad g(q, \tau) = A_1(q)(1 - f_1(q, \tau)) + A_2(q)(1 - f_2(q, \tau)) + B(q) \quad (6)$$

17  
18  
19  
20  
21 where indices 1 and 2 respectively correspond to the short-time (NPs contribution) and long-time  
22  
23 (aggregate/drift contribution) processes. We only considered the short-time diffusion coefficients  
24  
25  
26 in what follows.

27  
28  
29 In Figure 5.A, we express the evolution of the ISF  $f(q, \tau)$  as a function of the relaxation time  $\tau_R$   
30  
31 rescaled with the spatial frequency  $q^2$  to give insight of the dynamic process. This rescaling makes  
32  
33 the ISFs quantitatively comparable over variable  $q$ -ranges for all media considered, when  
34  
35 considering diffusive process with  $D = q^{-2} \tau_R^{-1}$ . These functions show the same dynamic processes  
36  
37 for NP-CEE-PEG<sub>HD</sub> and NP-PEG<sub>HD</sub> that decorrelate at  $\tau_R q^2 \sim 0.11 \text{ s}/\mu\text{m}^2$  ( $D \sim 8\text{-}9 \mu\text{m}^2/\text{s}$ ) in water  
38  
39 and at  $\tau_R q^2 \sim 0.71 \text{ s}/\mu\text{m}^2$  ( $D \sim 1.3\text{-}1.5 \mu\text{m}^2/\text{s}$ ) in Alg-Kcoil10%. However, in Alg-Kcoil20%, ISFs  
40  
41 corresponding to NP-CEE-PEG<sub>HD</sub> or NP-PEG<sub>HD</sub> do not overlap, indicating different diffusion  
42  
43 coefficient. In all cases, the stretching exponent,  $\beta$ , was found between 0.9 and 1, which implies  
44  
45 that no significant interaction between the NPs and the gels were observed in DDM.  
46  
47  
48

49  
50 From ISFs,  $\tau_R$  values were extracted to determine the diffusion coefficient of the NPs in both Alg-  
51  
52 Kcoil10% and Alg-Kcoil20% gels. Diffusion coefficients  $D$  were found independent of  $q$ ,  
53  
54 suggesting a diffusive motion within alginate gels as depicted in insets of Figure 5.A. The ratios  
55  
56  
57  
58  
59  
60

1  
2  
3 between diffusion coefficients of NPs measured in the gels,  $D$ , and in water,  $D_w$ , are presented in  
4  
5 Figure 5.B.  
6

7  
8 In Alg-Kcoil10%, no difference in  $D/D_w$  was observed between NP-CEE-PEG<sub>HD</sub> and NP-PEG<sub>HD</sub>:  
9  
10 both diffusion coefficients decreased to *ca.* 14% of the value that was obtained in water.  
11  
12 Interestingly, for NP-PEG<sub>HD</sub>, the  $D/D_w$  ratio increased from  $0.15 \pm 0.01$  in Alg-Kcoil10% to  $0.39$   
13  
14  $\pm 0.07$  in Alg-Kcoil20%. This could be due to differences in the structural properties of the  
15  
16 hydrogels. Indeed, Alg-Kcoil20% has a higher concentration of unreacted hydrophobic alkyne and  
17  
18 amphipathic Kcoil moieties than Alg-Kcoil10%.  
19  
20  
21  
22

23 A significant difference between particles was nonetheless observed in Alg-Kcoil20%, where the  
24  
25  $D/D_w$  of NP-CEE-PEG<sub>HD</sub> was found to be significantly lower than NP-PEG<sub>HD</sub> ( $D/D_w$  of  $0.25 \pm$   
26  
27  $0.01$  and  $0.39 \pm 0.07$ , respectively). This observation demonstrates that NP-CEE-PEG<sub>HD</sub> were  
28  
29 slowed down by a factor of 4 in Alg-Kcoil20% when compared to water, as opposed to a factor of  
30  
31 *ca.* 2.6 for NP-PEG<sub>HD</sub>. The data thus demonstrated that the specific interaction between Kcoil  
32  
33 (with sufficient concentration) and Cys-Ecoil-EGF had a significant impact on the diffusive  
34  
35 properties of nanoparticles.  
36  
37  
38  
39  
40  
41  
42  
43  
44  
45  
46  
47  
48  
49  
50  
51  
52  
53  
54  
55  
56  
57  
58  
59  
60

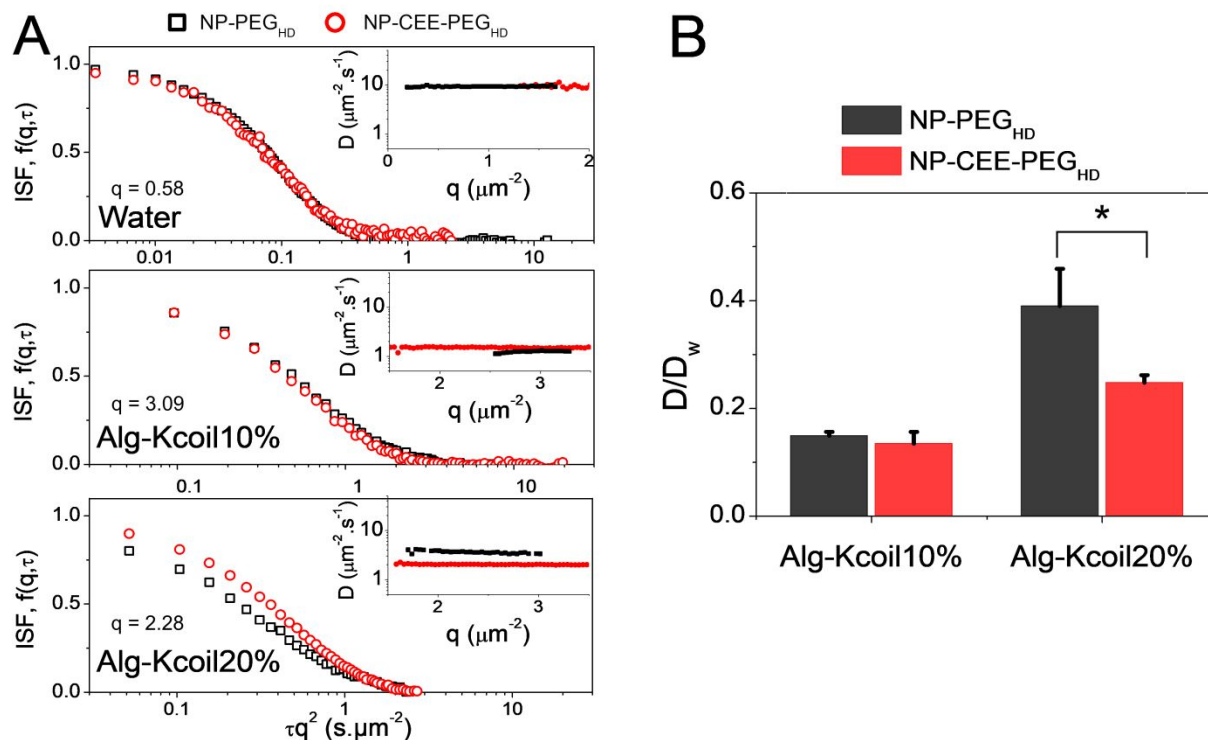


**Figure 5. Diffusive properties of NPs assessed by differential dynamic microscopy.** (A) Intermediate scattering function  $f(q, \tau) = \exp(-(\tau/\tau_r)^\beta)$  of NP-CEE-PEG<sub>HD</sub> (red circles) and NP-PEG<sub>HD</sub> (black squares) in water, Alg-Kcoil10% and Alg-Kcoil20%. In Alg-Kcoil10%, ISF were calculated using a double exponential as in Eq.6. Insets represent the coefficient diffusion  $D$  (averaged from 5 videos) vs  $q$  for each type of NPs. Different  $q$ -values were used for each medium to best represent the short-time plateau and the long-time plateau of the ISF. (B) Diffusion coefficients of NP-CEE-PEG<sub>HD</sub> and NP-PEG<sub>HD</sub>, as determined by DDM. The Y-axis represents the ratio between the coefficients of diffusion of NPs in the hydrogels,  $D$ , and in water,  $D_w$ . \* indicates statistical differences between datasets ( $n = 5$ ) (bilateral t-test,  $p < 0.05$ ).

### 3.4.2 NPs release from biofunctionalized hydrogels

The diffusive properties of the particles in hydrogels were further investigated in release studies. NP-CEE-PEG<sub>HD</sub> and NP-PEG<sub>HD</sub> particles were added to a 1% (total w/v) alginate solution containing 80-90% (w/v) of unmodified alginate supplemented with 10% of Alg-GPE, 10% of Alg-Kcoil or 20% of Alg-Kcoil, respectively referred to as Alg-Kcoil0%, Alg-Kcoil10% and Alg-

1  
2  
3 Kcoil20%. The solutions were poured in multiwell plates and gelled by the addition of CaCl<sub>2</sub> for  
4  
5 1 h. After gel formation, each gel was incubated in PBS. The concentration of AuNPs that were  
6  
7 released in the incubation medium was indirectly assessed at different timepoints by measuring  
8  
9 the number of NPs still entrapped in the hydrogels (Figure 6).  
10  
11

12  
13 As a starting point, we observed the release profiles of NP-PEG<sub>HD</sub> in different alginate medium.  
14  
15 We found that their release was slightly affected by the gel composition, where the higher the  
16  
17 Kcoil concentration was (from 0% to 10% and to 20%), the faster the NP-PEG<sub>HD</sub> particles were  
18  
19 released. This increase in release rate was observed since the first day, with respectively 68.4, 78.7  
20  
21 and 86.0% of NP-PEG<sub>HD</sub> released after 24 h, in qualitative agreement with the DDM results  
22  
23 (Figure 5). As mentioned, we ascribe this difference by the presence of Kcoil and/or the unreacted  
24  
25 alkyne moieties altering the structural properties (porosity) of the gel. Indeed, chains pending from  
26  
27 the alginate skeleton can affect crosslinking by preventing the alignment of the alginate chains and  
28  
29 thus the formation of the so-called “egg box” structure by which alginate crosslinks with calcium  
30  
31 cations.<sup>57</sup> The mechanical properties of the hydrogels were thus investigated using an indentation  
32  
33 assay. A decreasing trend between Alg-Kcoil0%, Alg-Kcoil10% and Alg-Kcoil20% was observed,  
34  
35 with Young’s modulus values of 360, 215 and 137, respectively. The data thus suggested that  
36  
37 mechanical cohesion of the gel decreased with an increasing amount of GPE content (see  
38  
39 Supplementary Information, Figure S1).  
40  
41  
42  
43  
44  
45

46 For NP-CEE-PEG<sub>HD</sub>, the general trend observed in the release profile studies was opposite to the  
47  
48 one obtained with NPs that bore PEG moieties only. Indeed, there was no increase of NP-CEE-  
49  
50 PEG<sub>HD</sub> release from Alg-Kcoil0% to Alg-Kcoil20% during the first 9 h. Moreover, after 24 h on,  
51  
52 the fraction of NP-CEE-PEG<sub>HD</sub> that was retained inside the gels was significantly higher in the  
53  
54 Alg-Kcoil20% hydrogel than in hydrogels with lower Kcoil content. More precisely, 42 ± 3 % of  
55  
56  
57  
58  
59  
60

1  
2  
3 the NP-CEE-PEG<sub>HD</sub> diffused out of the Alg-Kcoil20% hydrogel to the surrounding PBS medium  
4  
5 after 24 h, while  $63 \pm 4 \%$  and  $62 \pm 8 \%$  of the particles were released from Alg-Kcoil10% and  
6  
7 Alg-Kcoil0%, respectively (Figure 5). In Alg-Kcoil20% at 24 h, Ecoil-decorated nanoparticles,  
8  
9 NP-CEE-PEG<sub>HD</sub>, were retained twice as much as the nanoparticles with PEG only (42% and 86%  
10  
11 of release, respectively). Interestingly, there were no statistically significant differences between  
12  
13 NP-CEE-PEG<sub>HD</sub> and NP-PEG<sub>HD</sub> in Alg-Kcoil0% at any timepoint ( $n \geq 4$ ,  $p > 0.05$ ). This showed  
14  
15 that (a) the surface presentation of Cys-Ecoil-EGF had no detectable influence on NPs release in  
16  
17 absence of Kcoil and that (b) differences in NPs surface chemistry did not affect the structure of  
18  
19 the gel. The variations in release fraction between NP-PEG<sub>HD</sub> and NP-CEE-PEG<sub>HD</sub> in the Kcoil-  
20  
21 containing hydrogels could therefore not be attributed to CEE/alginate interactions but rather  
22  
23 confirmed that the surface presentation of the Ecoil-tagged protein hindered the mobility and  
24  
25 decreased the release of nanoparticles via the formation of the Ecoil/Kcoil complex.  
26  
27  
28  
29  
30  
31  
32  
33  
34  
35  
36  
37  
38  
39  
40  
41  
42  
43  
44  
45  
46  
47  
48  
49  
50  
51  
52  
53  
54  
55  
56  
57  
58  
59  
60

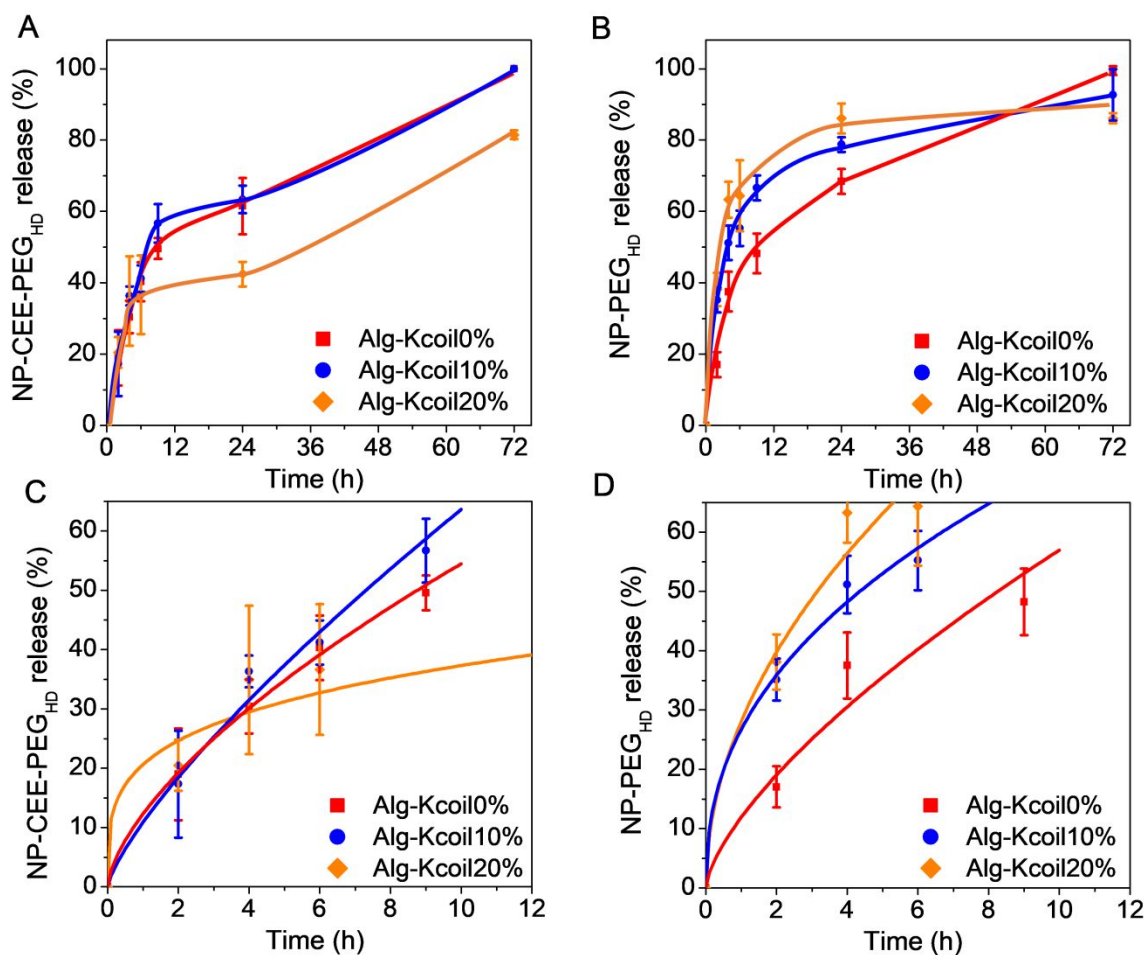


**Figure 6. NPs release from Kcoil-modified alginate hydrogels.** NP-CEE-PEG<sub>HD</sub> (A) and NP-PEG<sub>HD</sub> (B) are released from Alg-Kcoil0%, Alg-Kcoil10% and Alg-Kcoil20%, as calculated from the number of NPs still entrapped in the gel relative to  $t = 0$ . NP-CEE-PEG<sub>HD</sub> (C) and NP-PEG<sub>HD</sub> (D) data were fitted with a power-law model: each exponent was found to be between 0.43 and 1, characteristic of diffusion (both Fickian and non-Fickian), except for NP-CEE-PEG<sub>HD</sub> in Alg-Kcoil20%. ( $n \geq 4$ )

Altogether, the data revealed that the introduction of the Kcoil peptide in the hydrogel and its Ecoil partner on the nanoparticles slowed down the release of particles thanks to specific Ecoil/Kcoil interactions, despite conflicting changes in the bulk properties of the gel. So to understand the mechanism behind NP release, the experimental NPs release curves were fitted using a power-law model as described by Ritger and Peppas:<sup>58,59</sup>



$$y = kt^n, \quad (6)$$

where  $y$  is the fractional solute release,  $k$  is a constant,  $t$  the release time and  $n$  is the diffusional exponent. The fitted parameters are shown in Table 2.

In all but one case, diffusional exponents were found between 0.43 and 1, which is characteristic of a purely diffusive mechanism (0.43 being purely Fickian and ]0.43;1[ describing an anomalous transport, i.e. a mix of Fickian and non-Fickian diffusions). For NP-CEE-PEG<sub>HD</sub> in Alg-Kcoil20% only, a diffusional exponent  $n$  of 0.25 was calculated, which means that the power-law model cannot be applied and that the release mechanism cannot be explained by diffusion only. In that specific case, it was thus apparent that another mechanism was contributing to the release of the particles, most likely the specific Ecoil/Kcoil interaction.

It is also worth mentioning that the initial burst release of NP-CEE-PEG<sub>HD</sub> was both larger and longer in Alg-Kcoil10% (ca. 60% of total NPs between 0 and 9 h) than in Alg-Kcoil20% (ca. 40% of total NPs within 6 h, Figure 5.A). Following this burst, the behavior of the particles in all three gels was highly similar: little to no particle release from 12 to 24 h, then a slow and steady release with the same apparent rate between 24 and 72 h (36 to 39% of particle loss). The release rates measured after 24 h could be explained by gel erosion (which was noticed when manipulating the gels). Indeed, nanoparticles could be released along with the alginate chains whether they contained Kcoil moieties or not. This would have also occurred in hydrogels containing NP-PEG<sub>HD</sub>, even though it would have been difficult to observe given that the amount released at 24 h was already very high (ca. 85%). When comparing NP-CEE-PEG<sub>HD</sub> with NP-PEG<sub>HD</sub> in Alg-Kcoil20%, the release mechanism thus appeared as two-fold: first, a slow release of particles

decorated with Ecoil moieties only, thanks to Ecoil/Kcoil interactions, and second, gel erosion that caused the release of NP-CEE-PEG<sub>HD</sub> to catch up with the release of NP-PEG<sub>HD</sub>.

**Table 2:** Results of the fitting parameters obtained using Eq. 6

	<i>NP-CEE-PEG<sub>HD</sub></i>			<i>NP-PEG<sub>HD</sub></i>		
	n	k	R <sup>2</sup>	n	k	R <sup>2</sup>
<i>Alg-Kcoil0%</i>	0.65	0.12	1.00	0.68	0.12	0.89
<i>Alg-Kcoil10%</i>	0.77	0.11	0.96	0.43	0.27	0.95
<i>Alg-Kcoil20%</i>	0.26	0.21	0.72	0.50	0.28	0.89

n: exponent of the power-law, included between 0.43 and 1 for the model

k: multiplication factor of the Power Law

R<sup>2</sup>: determination coefficient of the fittings

Parameters were fitted using a linear regression on  $\ln(y) = f(\ln(t))$

Altogether, both DDM and release tests demonstrated that coiled-coil interactions have a significant impact on the diffusive properties of the nanoparticles in hydrogels by slowing their release, from the combination of the structure of the gel and coil interactions. DDM was found to be a useful predictor of the release flux of NPs in gels by characterizing their diffusion coefficient *D* and correlating it to actual release of NPs.

### 3.4.3 Bioactivity of released NPs

To assess the biological potency of the NPs that were first entrapped in gels then released in PBS (for a total of 72 h spent in the multiwell plate), an EGFR phosphorylation assay was conducted as previously described. The NP-CEE-PEG<sub>HD</sub> that were collected after their release showed a

1  
2  
3 strong phosphorylation induction, to an extent highly similar to fresh NPs and equivalent to 4.4  
4 nM of soluble EGF (to be compared with 4.9 nM for fresh particles, cf. Figure 3). This experiment  
5 highlighted that the bioactivity of the EGF moiety on the surface of the released NP remained  
6 unaffected by the trapping and release process, critical to achieve any desired therapeutic response.  
7 This further strengthened our confidence in coiled-coil affinity-based drug delivery system as  
8 versatile tool to deliver, in a timely manner, nanoparticles to a specific tissue, as here explored for  
9 cells expressing EGF receptors.  
10  
11  
12  
13  
14  
15  
16  
17  
18  
19  
20  
21  
22

## 23 4. Conclusions

24  
25  
26  
27  
28 Herein we report the use of coiled-coil interactions to extend the release rate of EGF-decorated  
29 gold nanoparticles from an alginate hydrogel. The proposed approach relies on the covalent  
30 grafting of the Ecoil peptide on NPs and its complementary partner, the Kcoil, on alginate chains.  
31 As a proof of concept, we showed that, when compared to AuNPs with PEG only, AuNPs  
32 decorated with both the Ecoil peptide and the epidermal growth factor were released more slowly  
33 from hydrogels that featured a high Kcoil peptide content. The released AuNPs were still able to  
34 induce EGFR-receptor activation via surface-grafted EGF.  
35  
36  
37  
38  
39  
40  
41  
42  
43  
44

45 To the best of our knowledge, we here showed for the first time that the delivery of a bioactive cue  
46 can be controlled by using an affinity-based hybrid system, that is, a nanoparticulate carrier  
47 entrapped within a hydrogel using specific affinity interactions. This strategy offers a wide range  
48 of applications. Gold NPs have indeed been widely used in photothermal therapy, radiotherapy,  
49 imaging and drug delivery. This system could also be applied to other types of nanoparticles (e.g.  
50  
51  
52  
53  
54  
55  
56  
57  
58  
59  
60

1  
2  
3 liposomes or polymeric NPs) for the delivery of either hydrophilic or hydrophobic drugs. Indeed,  
4  
5 the use of coiled-coil peptides provides a high level of versatility, as these peptides are highly  
6  
7 stable and can be grafted on virtually any molecule or structure. Moreover, the rationale design of  
8  
9 the peptide sequences should allow for a high level of tunability in the thermodynamics of the  
10  
11 interaction and therefore in the release rates of the therapeutics of interest.  
12  
13  
14  
15  
16  
17  
18  
19  
20  
21  
22  
23  
24  
25  
26

## 27 ASSOCIATED CONTENT

28  
29  
30

31 Supporting Information: Mechanical properties of alginate hydrogels (indentation assays) and  
32  
33 estimation of pore size.  
34  
35  
36  
37  
38  
39  
40  
41  
42  
43  
44  
45  
46  
47  
48  
49  
50  
51  
52  
53  
54  
55  
56  
57  
58  
59  
60

1  
2  
3 AUTHOR INFORMATION  
4  
5

6 Corresponding Authors  
7

8 \*E-mail: [gregory.decrescenzo@polymtl.ca](mailto:gregory.decrescenzo@polymtl.ca).  
9

10 \*E-mail: [xavier.banquy@umontreal.ca](mailto:xavier.banquy@umontreal.ca).  
11  
12  
13

14 AUTHOR CONTRIBUTIONS  
15

16 The manuscript was written through contributions of all authors.  
17  
18  
19

20 ORCID  
21  
22

23 Xavier Banquy: 0000-0002-3342-3179  
24

25 Gregory De Crescenzo: 0000-0002-6280-1570  
26

27 Frederic Murschel: 0000-0002-6735-8934  
28  
29

30 CONFLICTS OF INTEREST  
31  
32

33 The authors declare no competing financial interest.  
34  
35

36 ACKNOWLEDGMENT  
37  
38

39 This work was supported by the Canada Research Chairs on Protein-enhanced Biomaterials  
40 (G.D.C.) and on Bioinspired Materials (X.B.), by the Natural Sciences and Engineering Research  
41 Council of Canada Discovery Grant (P.L.L., G.D.C. and X.B.), by the Biomedical Science and  
42 Technology Research Group (B.L., F.M., and G.D.C.) and the Fonds de Recherche du Québec –  
43 Nature et Technologies (F.M.). V.A.M. acknowledges financial support from a ERC-2013-AdG  
44 340877-PHYSAPS. The present work was funded by the TransMedTech Institute (B.L. and F.M.)  
45 and its main funding partner, the Canada First Research Excellence Fund. We would like to thank  
46 S. Bilodeau for NMR measurements and C. Ribeiro for ELISA assay.  
47  
48  
49  
50  
51  
52  
53  
54  
55  
56  
57  
58  
59  
60

## REFERENCES

- 1  
2  
3  
4  
5  
6 (1) El-Say, K. M.; El-Sawy, H. S. Polymeric Nanoparticles: Promising Platform for Drug  
7 Delivery. *Int. J. Pharmaceut.* **2017**, *528* (1), 675–691.  
8 <https://doi.org/10.1016/j.ijpharm.2017.06.052>.
- 9 (2) Hassan, S.; Prakash, G.; Bal Ozturk, A.; Saghadzadeh, S.; Farhan Sohail, M.; Seo, J.; Remzi  
10 Dokmeci, M.; Zhang, Y. S.; Khademhosseini, A. Evolution and Clinical Translation of Drug  
11 Delivery Nanomaterials. *Nano Today* **2017**, *15*, 91–106.  
12 <https://doi.org/10.1016/j.nantod.2017.06.008>.
- 13 (3) Vulic, K.; Shoichet, M. S. Affinity-Based Drug Delivery Systems for Tissue Repair and  
14 Regeneration. *Biomacromolecules* **2014**, *15* (11), 3867–3880.  
15 <https://doi.org/10.1021/bm501084u>.
- 16 (4) Kakkar, A.; Traverso, G.; Farokhzad, O. C.; Weissleder, R.; Langer, R. Evolution of  
17 Macromolecular Complexity in Drug Delivery Systems. *Nat. Rev. Chem.* **2017**, *1* (8), 0063.  
18 <https://doi.org/10.1038/s41570-017-0063>.
- 19 (5) Delplace, V.; Obermeyer, J.; Shoichet, M. S. Local Affinity Release. *ACS Nano* **2016**, *10*  
20 (7), 6433–6436. <https://doi.org/10.1021/acsnano.6b04308>.
- 21 (6) Freeman, I.; Cohen, S. The Influence of the Sequential Delivery of Angiogenic Factors from  
22 Affinity-Binding Alginate Scaffolds on Vascularization. *Biomaterials* **2009**, *30* (11), 2122–  
23 2131. <https://doi.org/10.1016/j.biomaterials.2008.12.057>.
- 24 (7) Lin, C.-C.; Anseth, K. S. Controlling Affinity Binding with Peptide-Functionalized  
25 Poly(Ethylene Glycol) Hydrogels. *Adv. Funct. Mater.* **2009**, *19* (14), 2325.  
26 <https://doi.org/10.1002/adfm.200900107>.
- 27 (8) Battig, M. R.; Soontornworajit, B.; Wang, Y. Programmable Release of Multiple Protein  
28 Drugs from Aptamer-Functionalized Hydrogels via Nucleic Acid Hybridization. *J. Am.*  
29 *Chem. Soc.* **2012**, *134* (30), 12410–12413. <https://doi.org/10.1021/ja305238a>.
- 30 (9) Mulyasmita, W.; Cai, L.; Hori, Y.; Heilshorn, S. C. Avidity-Controlled Delivery of  
31 Angiogenic Peptides from Injectable Molecular-Recognition Hydrogels. *Tissue Eng. Part*  
32 *A* **2014**, *20* (15–16), 2102–2114. <https://doi.org/10.1089/ten.tea.2013.0357>.
- 33 (10) Thatiparti, T. R.; Shoffstall, A. J.; von Recum, H. A. Cyclodextrin-Based Device Coatings  
34 for Affinity-Based Release of Antibiotics. *Biomaterials* **2010**, *31* (8), 2335–2347.  
35 <https://doi.org/10.1016/j.biomaterials.2009.11.087>.
- 36 (11) J. Webber, M.; Langer, R. Drug Delivery by Supramolecular Design. *Chem. Soc. Rev.* **2017**,  
37 *46* (21), 6600–6620. <https://doi.org/10.1039/C7CS00391A>.
- 38 (12) Cheng, H.; Chawla, A.; Yang, Y.; Li, Y.; Zhang, J.; Jang, H. L.; Khademhosseini, A.  
39 Development of Nanomaterials for Bone-Targeted Drug Delivery. *Drug Disc. Today* **2017**,  
40 *22* (9), 1336–1350. <https://doi.org/10.1016/j.drudis.2017.04.021>.
- 41 (13) Vermonden, T.; Censi, R.; Hennink, W. E. Hydrogels for Protein Delivery. *Chem. Rev.*  
42 **2012**, *112* (5), 2853–2888. <https://doi.org/10.1021/cr200157d>.
- 43 (14) Rambhia, K. J.; Ma, P. X. Controlled Drug Release for Tissue Engineering. *J. Controlled*  
44 *Release* **2015**, *219*, 119–128. <https://doi.org/10.1016/j.jconrel.2015.08.049>.
- 45 (15) Parry, D. A. D.; Fraser, R. D. B.; Squire, J. M. Fifty Years of Coiled-Coils and Alpha-  
46 Helical Bundles: A Close Relationship between Sequence and Structure. *J. Struct. Biol.*  
47 **2008**, *163* (3), 258–269. <https://doi.org/10.1016/j.jsb.2008.01.016>.
- 48  
49  
50  
51  
52  
53  
54  
55  
56  
57  
58  
59  
60

- 1  
2  
3  
4  
5  
6  
7  
8  
9  
10  
11  
12  
13  
14  
15  
16  
17  
18  
19  
20  
21  
22  
23  
24  
25  
26  
27  
28  
29  
30  
31  
32  
33  
34  
35  
36  
37  
38  
39  
40  
41  
42  
43  
44  
45  
46  
47  
48  
49  
50  
51  
52  
53  
54  
55  
56  
57  
58  
59  
60
- (16) Apostolovic, B.; Danial, M.; Klok, H.-A. Coiled Coils: Attractive Protein Folding Motifs for the Fabrication of Self-Assembled, Responsive and Bioactive Materials. *Chem. Soc. Rev.* **2010**, *39* (9), 3541–3575. <https://doi.org/10.1039/b914339b>.
- (17) Eskandari, S.; Guerin, T.; Toth, I.; Stephenson, R. J. Recent Advances in Self-Assembled Peptides: Implications for Targeted Drug Delivery and Vaccine Engineering. *Adv. Drug Deliv. Rev.* **2017**, *110–111*, 169–187. <https://doi.org/10.1016/j.addr.2016.06.013>.
- (18) Wu, Y.; Collier, J. H.  $\alpha$ -Helical Coiled-Coil Peptide Materials for Biomedical Applications. *Wiley Interdiscip. Rev. Nanomed. Nanobiotechnol.* **2017**, *9* (2), e1424. <https://doi.org/10.1002/wnan.1424>.
- (19) Pechar, M.; Pola, R.; Laga, R.; Ulbrich, K.; Bednárová, L.; Maloň, P.; Siegllová, I.; Král, V.; Fábry, M.; Vaněk, O. Coiled Coil Peptides as Universal Linkers for the Attachment of Recombinant Proteins to Polymer Therapeutics. *Biomacromolecules* **2011**, *12* (10), 3645–3655. <https://doi.org/10.1021/bm200897b>.
- (20) Assal, Y.; Mizuguchi, Y.; Mie, M.; Kobatake, E. Growth Factor Tethering to Protein Nanoparticles via Coiled-Coil Formation for Targeted Drug Delivery. *Bioconjugate Chem.* **2015**, *26* (8), 1672–1677. <https://doi.org/10.1021/acs.bioconjchem.5b00266>.
- (21) Siew, S.; Kaneko, M.; Mie, M.; Kobatake, E. Construction of a Tissue-Specific Transcription Factor-Tethered Extracellular Matrix Protein via Coiled-Coil Helix Formation. *J. Mater. Chem. B* **2016**, *4* (14), 2512–2518. <https://doi.org/10.1039/C5TB01579K>.
- (22) Noel, S.; Fortier, C.; Murschel, F.; Belzil, A.; Gaudet, G.; Jolicoeur, M.; De Crescenzo, G. Co-Immobilization of Adhesive Peptides and VEGF within a Dextran-Based Coating for Vascular Applications. *Acta Biomater.* **2016**, *37*, 69–82. <https://doi.org/10.1016/j.actbio.2016.03.043>.
- (23) De Crescenzo, G.; Litowski, J. R.; Hodges, R. S.; O'Connor-McCourt, M. D. Real-Time Monitoring of the Interactions of Two-Stranded de Novo Designed Coiled-Coils: Effect of Chain Length on the Kinetic and Thermodynamic Constants of Binding. *Biochemistry* **2003**, *42* (6), 1754–1763. <https://doi.org/10.1021/bi0268450>.
- (24) Murschel, F.; Fortier, C.; Jolicoeur, M.; Hodges, R. S.; De Crescenzo, G. Two Complementary Approaches for the Controlled Release of Biomolecules Immobilized via Coiled-Coil Interactions: Peptide Core Mutations and Multivalent Presentation. *Biomacromolecules* **2017**, *18* (3), 965–975. <https://doi.org/10.1021/acs.biomac.6b01830>.
- (25) Litowski, J. R.; Hodges, R. S. Designing Heterodimeric Two-Stranded  $\alpha$ -Helical Coiled-Coils: The Effect of Chain Length on Protein Folding, Stability and Specificity. *The Journal of Peptide Research* **2001**, *58* (6), 477–492. <https://doi.org/10.1034/j.1399-3011.2001.10972.x>.
- (26) Her, S.; Jaffray, D. A.; Allen, C. Gold Nanoparticles for Applications in Cancer Radiotherapy: Mechanisms and Recent Advancements. *Adv. Drug Deliv. Rev.* **2017**, *109*, 84–101. <https://doi.org/10.1016/j.addr.2015.12.012>.
- (27) Riley, R. S.; Day, E. S. Gold Nanoparticle-Mediated Photothermal Therapy: Applications and Opportunities for Multimodal Cancer Treatment. *Wiley Interdiscip. Rev. Nanomed. Nanobiotechnol.* **2017**, *9* (4), e1449. <https://doi.org/10.1002/wnan.1449>.
- (28) Kong, F.-Y.; Zhang, J.-W.; Li, R.-F.; Wang, Z.-X.; Wang, W.-J.; Wang, W. Unique Roles of Gold Nanoparticles in Drug Delivery, Targeting and Imaging Applications. *Molecules* **2017**, *22* (9), 1445. <https://doi.org/10.3390/molecules22091445>.

- 1  
2  
3 (29) Agüero, L.; Zaldivar-Silva, D.; Peña, L.; Dias, M. L. Alginate Microparticles as Oral Colon  
4 Drug Delivery Device: A Review. *Carbohydr. Polym.* **2017**, *168*, 32–43.  
5 <https://doi.org/10.1016/j.carbpol.2017.03.033>.  
6  
7 (30) Zhao, F.; Yao, D.; Guo, R.; Deng, L.; Dong, A.; Zhang, J. Composites of Polymer Hydrogels  
8 and Nanoparticulate Systems for Biomedical and Pharmaceutical Applications.  
9 *Nanomaterials (Basel)* **2015**, *5* (4), 2054–2130. <https://doi.org/10.3390/nano5042054>.  
10  
11 (31) Mauri, E.; Papa, S.; Masi, M.; Veglianese, P.; Rossi, F. Novel Functionalization Strategies  
12 to Improve Drug Delivery from Polymers. *Expert Opin. Drug Deliv.* **2017**, *14* (11), 1305–  
13 1313. <https://doi.org/10.1080/17425247.2017.1285280>.  
14  
15 (32) Riahi, N.; Murschel, F.; Lerouge, S.; Durocher, Y.; Henry, O.; De Crescenzo, G.  
16 Bioavailability of Immobilized Epidermal Growth Factor: Covalent versus Noncovalent  
17 Grafting. *Biointerphases* **2017**, *12* (1), 010501. <https://doi.org/10.1116/1.4978871>.  
18  
19 (33) Kumar, S.; Aaron, J.; Sokolov, K. Directional Conjugation of Antibodies to Nanoparticles  
20 for Synthesis of Multiplexed Optical Contrast Agents with Both Delivery and Targeting  
21 Moieties. *Nature Protocols* **2008**, *3* (2), 314–320. <https://doi.org/10.1038/nprot.2008.1>.  
22  
23 (34) Hinterwirth, H.; Kappel, S.; Waitz, T.; Prohaska, T.; Lindner, W.; Lämmerhofer, M.  
24 Quantifying Thiol Ligand Density of Self-Assembled Monolayers on Gold Nanoparticles  
25 by Inductively Coupled Plasma–Mass Spectrometry. *ACS Nano* **2013**, *7* (2), 1129–1136.  
26 <https://doi.org/10.1021/nn306024a>.  
27  
28 (35) Liu, X.; Atwater, M.; Wang, J.; Huo, Q. Extinction Coefficient of Gold Nanoparticles with  
29 Different Sizes and Different Capping Ligands. *Colloids Surf. B Biointerfaces* **2007**, *58* (1),  
30 3–7. <https://doi.org/10.1016/j.colsurfb.2006.08.005>.  
31  
32 (36) Smith, A. M.; Marbella, L. E.; Johnston, K. A.; Hartmann, M. J.; Crawford, S. E.; Kozycz,  
33 L. M.; Seferos, D. S.; Millstone, J. E. Quantitative Analysis of Thiolated Ligand Exchange  
34 on Gold Nanoparticles Monitored by <sup>1</sup>H NMR Spectroscopy. *Anal. Chem.* **2015**, *87* (5),  
35 2771–2778. <https://doi.org/10.1021/ac504081k>.  
36  
37 (37) Murschel, F.; Liberelle, B.; St-Laurent, G.; Jolicoeur, M.; Durocher, Y.; De Crescenzo, G.  
38 Coiled-Coil-Mediated Grafting of Bioactive Vascular Endothelial Growth Factor. *Acta*  
39 *Biomaterialia* **2013**, *9* (6), 6806–6813. <https://doi.org/10.1016/j.actbio.2013.02.032>.  
40  
41 (38) Spellman, D.; McEvoy, E.; O’Cuinn, G.; FitzGerald, R. J. Proteinase and Exopeptidase  
42 Hydrolysis of Whey Protein: Comparison of the TNBS, OPA and PH Stat Methods for  
43 Quantification of Degree of Hydrolysis. *International Dairy Journal*. 13th ed. 2003, pp  
44 447–453.  
45  
46 (39) Noel, S.; Liberelle, B.; Robitaille, L.; De Crescenzo, G. Quantification of Primary Amine  
47 Groups Available for Subsequent Biofunctionalization of Polymer Surfaces. *Bioconjug.*  
48 *Chem.* **2011**, *22* (8), 1690–1699. <https://doi.org/10.1021/bc200259c>.  
49  
50 (40) Cerbino, R.; Trappe, V. Differential Dynamic Microscopy: Probing Wave Vector  
51 Dependent Dynamics with a Microscope. *Phys. Rev. Lett.* **2008**, *100* (18), 188102.  
52 <https://doi.org/10.1103/PhysRevLett.100.188102>.  
53  
54 (41) Edera, P.; Bergamini, D.; Trappe, V.; Giavazzi, F.; Cerbino, R. Differential Dynamic  
55 Microscopy Microrheology of Soft Materials: A Tracking-Free Determination of the  
56 Frequency-Dependent Loss and Storage Moduli. *Phys. Rev. Materials* **2017**, *1* (7), 073804.  
57 <https://doi.org/10.1103/PhysRevMaterials.1.073804>.  
58  
59 (42) Escobedo-Sánchez, M. A.; Segovia-Gutiérrez, J. P.; Zuccolotto-Bernez, A. B.; Hansen, J.;  
60 Marciniak, C. C.; Sachowsky, K.; Platten, F.; Egelhaaf, S. U. Microliter Viscometry Using

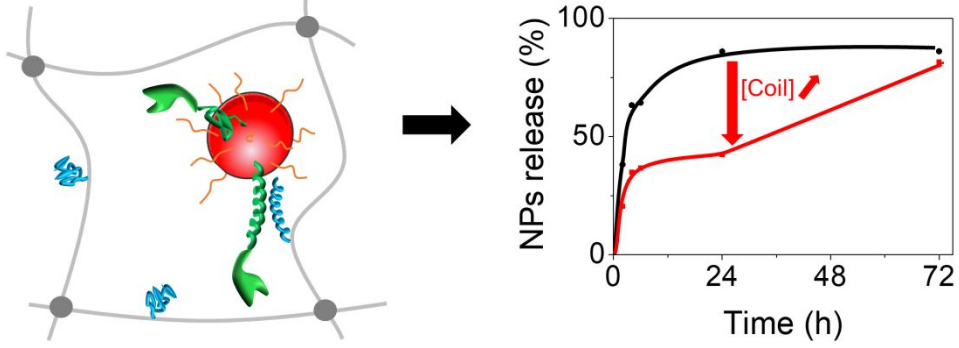


- a Bright-Field Microscope:  $\eta$ -DDM. *Soft Matter* **2018**, *14* (34), 7016–7025. <https://doi.org/10.1039/C8SM00784E>.
- (43) Martinez, V. A.; Schwarz-Linek, J.; Reufer, M.; Wilson, L. G.; Morozov, A. N.; Poon, W. C. K. Flagellated Bacterial Motility in Polymer Solutions. *PNAS* **2014**, *111* (50), 17771–17776. <https://doi.org/10.1073/pnas.1415460111>.
- (44) Martinez, V. A.; Besseling, R.; Croze, O. A.; Tailleur, J.; Reufer, M.; Schwarz-Linek, J.; Wilson, L. G.; Bees, M. A.; Poon, W. C. K. Differential Dynamic Microscopy: A High-Throughput Method for Characterizing the Motility of Microorganisms. *Biophys. J.* **2012**, *103* (8), 1637–1647. <https://doi.org/10.1016/j.bpj.2012.08.045>.
- (45) Reufer, M.; Martinez, V. A.; Schurtenberger, P.; Poon, W. C. K. Differential Dynamic Microscopy for Anisotropic Colloidal Dynamics. *Langmuir* **2012**, *28* (10), 4618–4624. <https://doi.org/10.1021/la204904a>.
- (46) Wilson, L. G.; Martinez, V. A.; Schwarz-Linek, J.; Tailleur, J.; Bryant, G.; Pusey, P. N.; Poon, W. C. K. Differential Dynamic Microscopy of Bacterial Motility. *Phys. Rev. Lett.* **2011**, *106* (1), 018101. <https://doi.org/10.1103/PhysRevLett.106.018101>.
- (47) Boucher, C.; St-Laurent, G.; Loignon, M.; Jolicoeur, M.; De Crescenzo, G.; Durocher, Y. The Bioactivity and Receptor Affinity of Recombinant Tagged EGF Designed for Tissue Engineering Applications Is Defined by the Nature and Position of the Tags. *Tissue Eng. Part A* **2008**, *14* (12), 2069–2077. <https://doi.org/10.1089/ten.tea.2008.0037>.
- (48) Rahme, K.; Chen, L.; Hobbs, R. G.; Morris, M. A.; O'Driscoll, C.; Holmes, J. D. PEGylated Gold Nanoparticles: Polymer Quantification as a Function of PEG Lengths and Nanoparticle Dimensions. *RSC Adv.* **2013**, *3* (17), 6085–6094. <https://doi.org/10.1039/C3RA22739A>.
- (49) Boon, J. P.; Nossal, R.; Chen, S.-H. Light-Scattering Spectrum Due to Wiggling Motions of Bacteria. *Biophys. J.* **1974**, *14* (11), 847–864.
- (50) Song, L.; Falzone, N.; Vallis, K. A. EGF-Coated Gold Nanoparticles Provide an Efficient Nano-Scale Delivery System for the Molecular Radiotherapy of EGFR-Positive Cancer. *Int. J. Radiat. Biol.* **2016**, *92* (11), 716–723. <https://doi.org/10.3109/09553002.2016.1145360>.
- (51) Yarden, Y.; Harari, I.; Schlessinger, J. Purification of an Active EGF Receptor Kinase with Monoclonal Antireceptor Antibodies. *J. Biol. Chem.* **1985**, *260* (1), 315–319.
- (52) Liberelle, B.; Boucher, C.; Chen, J.; Jolicoeur, M.; Durocher, Y.; De Crescenzo, G. Impact of Epidermal Growth Factor Tethering Strategy on Cellular Response. *Bioconjug. Chem.* **2010**, *21* (12), 2257–2266. <https://doi.org/10.1021/bc1002604>.
- (53) Nielsen, T. T.; Wintgens, V.; Amiel, C.; Wimmer, R.; Larsen, K. L. Facile Synthesis of  $\beta$ -Cyclodextrin-Dextran Polymers by “Click” Chemistry. *Biomacromolecules* **2010**, *11* (7), 1710–1715. <https://doi.org/10.1021/bm9013233>.
- (54) Kinh, C. D.; Thien, T. V.; Hoa, T. T.; Khieu, D. Q. Interpretation of <sup>1</sup>H-NMR Spectrum of Alginate by <sup>1</sup>H-<sup>1</sup>H TOCSY and COSY Spectrum. *Viet. J. Chem.* **2007**, *45* (6), 772.
- (55) Engler, A. C.; Lee, H.; Hammond, P. T. Highly Efficient “Grafting onto” a Polypeptide Backbone Using Click Chemistry. *Angew. Chem. Int. Ed.* **2009**, *48* (49), 9334–9338. <https://doi.org/10.1002/anie.200904070>.
- (56) Patel, K. G.; Swartz, J. R. Surface Functionalization of Virus-Like Particles by Direct Conjugation Using Azide–Alkyne Click Chemistry. *Bioconjug. Chem.* **2011**, *22* (3), 376–387. <https://doi.org/10.1021/bc100367u>.

- 1  
2  
3 (57) Grant, G. T.; Morris, E. R.; Rees, D. A.; Smith, P. J. C.; Thom, D. Biological Interactions  
4 between Polysaccharides and Divalent Cations: The Egg-Box Model. *FEBS Lett.* **1973**, *32*  
5 (1), 195–198. [https://doi.org/10.1016/0014-5793\(73\)80770-7](https://doi.org/10.1016/0014-5793(73)80770-7).  
6  
7 (58) Ritger, P. L.; Peppas, N. A. A Simple Equation for Description of Solute Release II. Fickian  
8 and Anomalous Release from Swellable Devices. *J. Controlled Release* **1987**, *5* (1), 37–42.  
9 [https://doi.org/10.1016/0168-3659\(87\)90035-6](https://doi.org/10.1016/0168-3659(87)90035-6).  
10 (59) Ritger, P. L.; Peppas, N. A. A Simple Equation for Description of Solute Release I. Fickian  
11 and Non-Fickian Release from Non-Swellable Devices in the Form of Slabs, Spheres,  
12 Cylinders or Discs. *J. Controlled Release* **1987**, *5* (1), 23–36. [https://doi.org/10.1016/0168-](https://doi.org/10.1016/0168-3659(87)90034-4)  
13 [3659\(87\)90034-4](https://doi.org/10.1016/0168-3659(87)90034-4).  
14  
15  
16  
17  
18  
19  
20  
21  
22  
23  
24  
25  
26  
27  
28  
29  
30  
31  
32  
33  
34  
35  
36  
37  
38  
39  
40  
41  
42  
43  
44  
45  
46  
47  
48  
49  
50  
51  
52  
53  
54  
55  
56  
57  
58  
59  
60

TABLE OF CONTENTS GRAPHIC

Coiled-coil affinity peptides for controlled release of nanoparticles



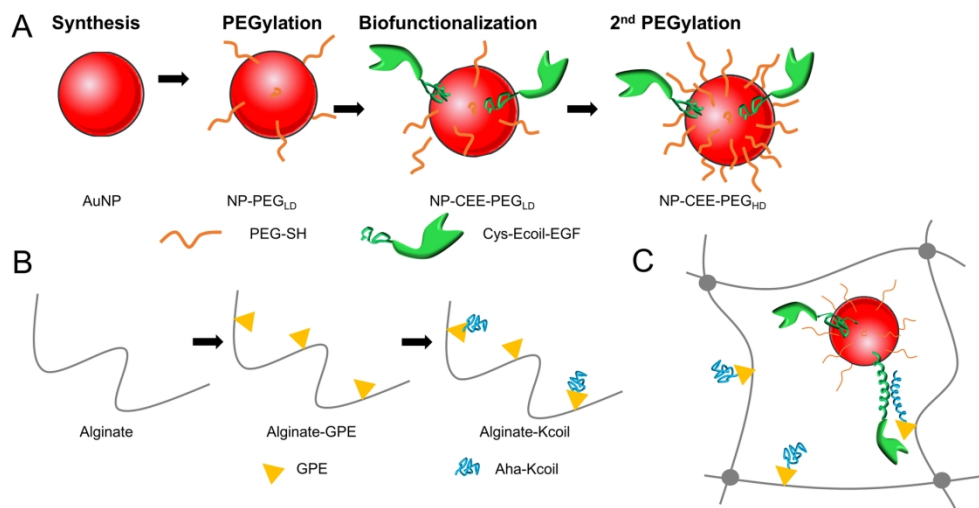


Figure 1. Preparation of the affinity-based hybrid system using gold nanoparticles and an alginate scaffold.

(A) AuNPs were first PEGylated to a low level for stabilization. Cys-Ecoil-EGF (CEE) was then grafted via thiol-gold chemistry. A second PEGylation step was then performed for higher stability. (B) Alginate chains were first derivatized with an alkyne moiety using glycidyl propargyl ether (GPE). Azidohomoalanine-tagged Kcoil peptides (Aha-Kcoil) were then grafted via azide-alkyne click chemistry. (C) The dispersion of Ecoil-AuNPs in the Kcoil-alginate hydrogel enabled the formation of the E/K coiled-coil complex to slow down NPs release.

169x90mm (300 x 300 DPI)

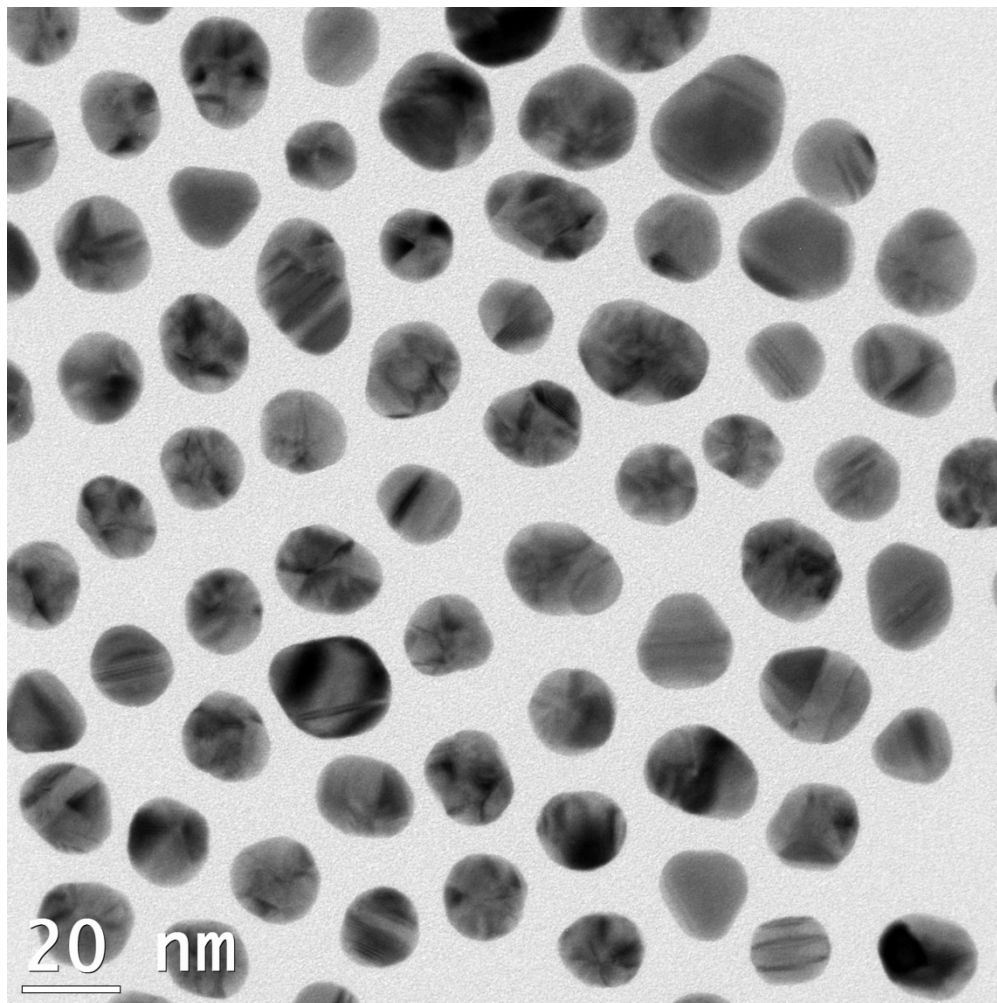


Figure 2 : Transmission electron microscopy (TEM) image of AuNPs.  
The average NPs diameter measured was  $18 \pm 2$  nm ( $n=100$ ).

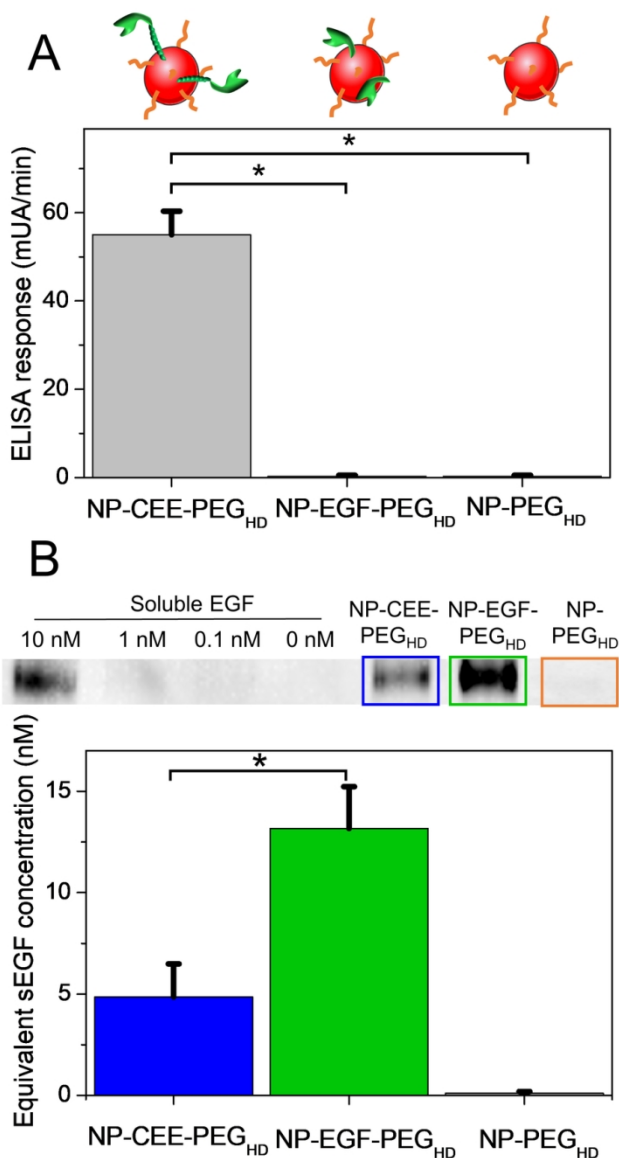


Figure 3. Bioadhesion and bioactivity of functionalized NPs.

(A) Bioadhesion on a Kcoil-derivatized surface of NP-CEE-PEG<sub>HD</sub>, NP-EGF-PEG<sub>HD</sub>, and NP-PEG<sub>HD</sub> as control, as detected by anti-EGF ELISA (n=3) (B) EGFR phosphorylation in A431 cells upon binding with soluble EGF (10, 1, 0.1 and 0 nM), NP-CEE-PEG<sub>HD</sub> or NP-EGF-PEG<sub>HD</sub> (EGF concentration of 1.5 nM according to ELISA) and NP-PEG<sub>HD</sub>, as monitored by Western Blot. The 180-kDa band immunoreactive to anti-phosphotyrosine antibodies (corresponding to EGFR) was quantified using a ChemiDoc and Image Lab software. Y-axis represents the equivalent concentration in soluble EGF (sEGF) (n = 3 for NP-CEE-PEG<sub>HD</sub> and NP-EGF-PEG<sub>HD</sub> and n = 1 for NP-PEG<sub>HD</sub>, \* indicates statistical differences between datasets (bilateral t-test, p < 0.05).

82x149mm (300 x 300 DPI)

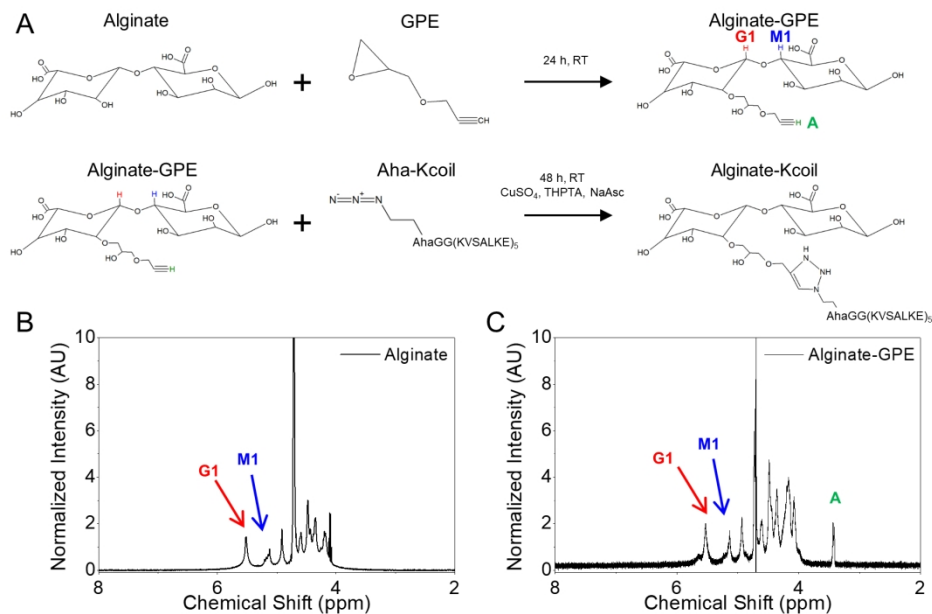


Figure 4. Synthesis and characterization of Kcoil-derivatized alginate.

(A) Alginate was first modified with glycidyl propargyl ether (GPE). Azide-terminated Kcoil peptides were then grafted on alginate-GPE via alkyne-azide click chemistry in presence of copper sulfate. (B and C) The percentage of alkyne-modified monomers was quantified by <sup>1</sup>H NMR using the peak at 3.4 ppm (peak A), corresponding to the alkyne, and the peaks at 5.5 ppm (G1) and 5.1 ppm (M1) as reference, corresponding to the total amount of monomers.

170x104mm (300 x 300 DPI)

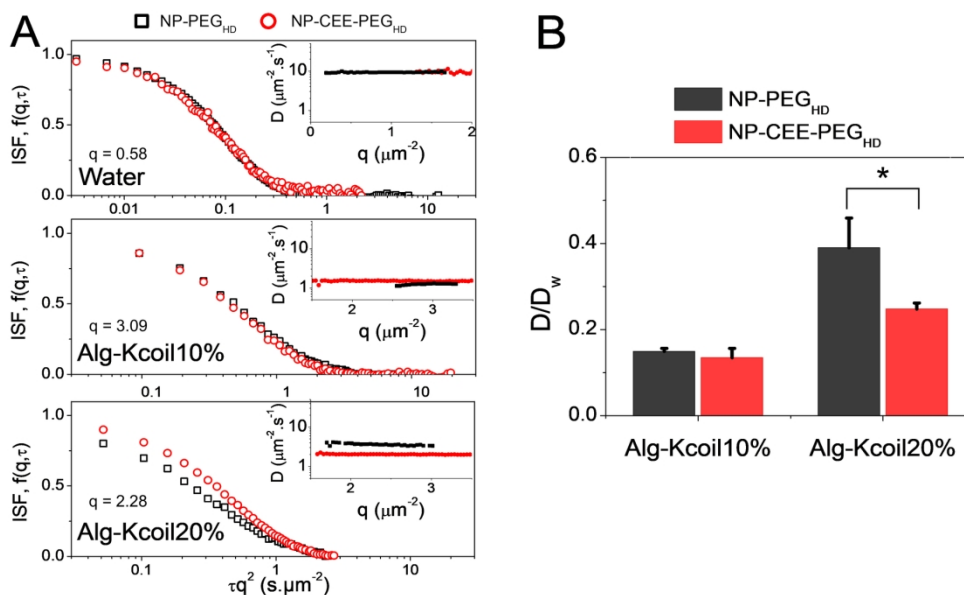


Figure 5. Diffusive properties of NPs assessed by differential dynamic microscopy. (A) Intermediate scattering function  $f(q, \tau) = \exp(-(\tau/\tau_R)\beta)$  of NP-CEE-PEG<sub>HD</sub> (red circles) and NP-PEG<sub>HD</sub> (black squares) in water, Alg-Kcoil10% and Alg-Kcoil20%. In Alg-Kcoil10%, ISF were calculated using a double exponential as in Eq.6. Insets represent the coefficient diffusion  $D$  (averaged from 5 videos) vs  $q$  for each type of NPs. Different  $q$ -values were used for each medium to best represent the short-time plateau and the long-time plateau of the ISF. (B) Diffusion coefficients of NP-CEE-PEG<sub>HD</sub> and NP-PEG<sub>HD</sub>, as determined by DDM. The Y-axis represents the ratio between the coefficients of diffusion of NPs in the hydrogels,  $D$ , and in water,  $D_w$ . \* indicates statistical differences between datasets ( $n = 5$ ) (bilateral t-test,  $p < 0.05$ ).

170x104mm (300 x 300 DPI)



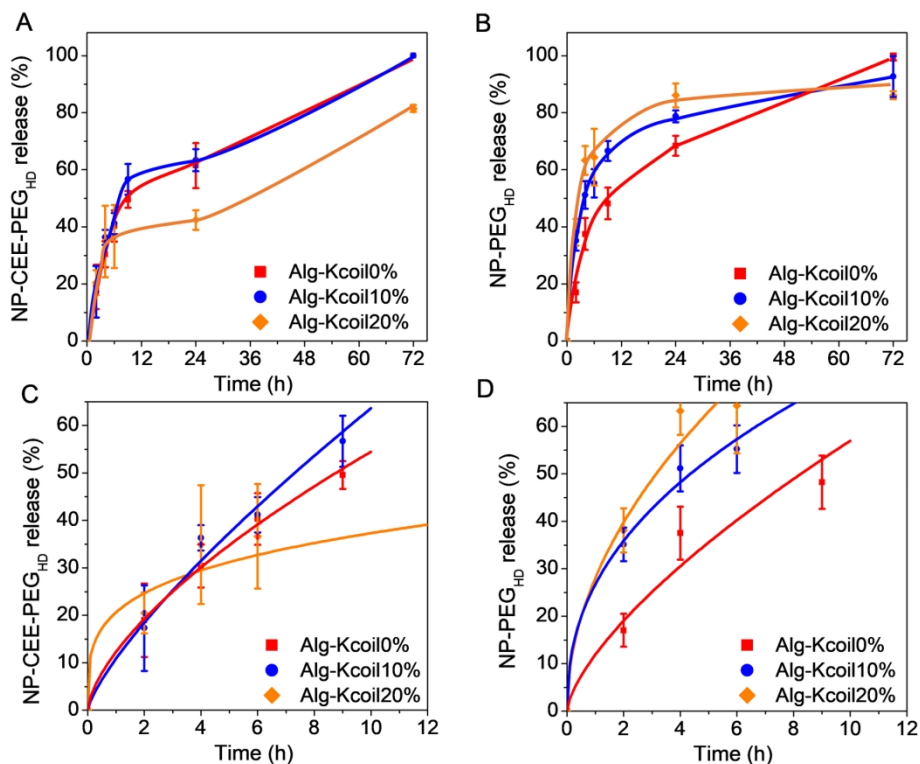
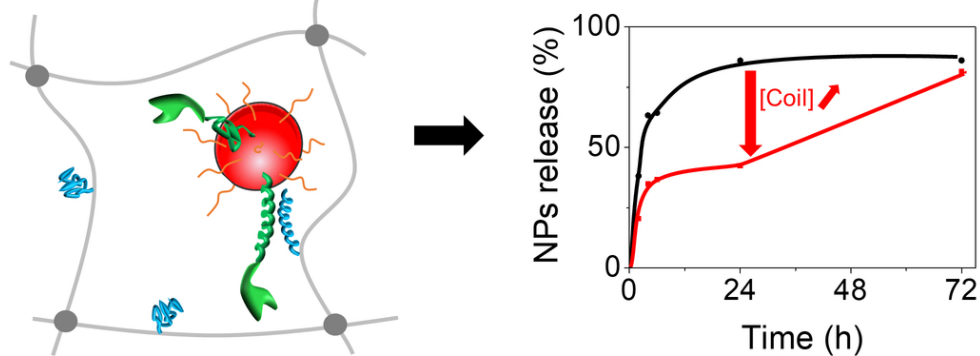


Figure 6. NPs release from Kcoil-modified alginate hydrogels. NP-CEE-PEG<sub>HD</sub> (A) and NP-PEG<sub>HD</sub> (B) are released from Alg-Kcoil0%, Alg-Kcoil10% and Alg-Kcoil20%, as calculated from the number of NPs still entrapped in the gel relative to  $t = 0$ . NP-CEE-PEG<sub>HD</sub> (C) and NP-PEG<sub>HD</sub> (D) data were fitted with a power-law model: each exponent was found to be between 0.43 and 1, characteristic of diffusion (both Fickian and non-Fickian), except for NP-CEE-PEG<sub>HD</sub> in Alg-Kcoil20%. ( $n \geq 4$ )

170x137mm (300 x 300 DPI)

Coiled-coil affinity peptides for controlled release of nanoparticles



Graphic for Table of Content

88x35mm (300 x 300 DPI)